PHYSICS BEYOND THE STANDARD MODEL: MASSIVE NEUTRINOS, SPIN 3/2 QUARKS

By

STEPHEN C. GIBBONS

Master of Science

Wichita State University

Wichita, Kansas

1990

Submitted to the Faculty of the
Graduate College of the
Oklahoma State University
in partial fulfillment of
the requirements for
the Degree of
DOCTOR OF PHILOSOPHY
May, 1999

PHYSICS BEYOND THE STANDARD MODEL:
MASSIVE NEUTRINOS, SPIN 3/2 QUARKS

Thesis Approved:

Satyanarayan Nanda 4/23/99
Thesis Adviser

Dean of the Graduate College

ACKNOWLEDGMENTS

I want to thank my advisor Dr. Satyanarayan Nandi for his kindness and his ability to teach. He not only provided the guidence I needed to accomplish my learning at OSU but he helped make my learning experience an enjoyable one. There are other Professors at OSU whom I admire too. I've never seen anyone as committed to his students as Dr. Paul Weshaus. And Dr. Mark Samuel, now deceased, was always an encouragement and brightened everyone's day with his friendly disposition. These faculty, and others, helped make OSU a good experience for me. Also, my officemates, Eric Steinfelds, Dave Muller, Bhaskar Dutta, Tesfaye Abraha, Jack Huesman, Danaiel Dumitru, and Chris McMullen were great people to know and work with. I'd like to give special thanks to Dave Muller for helping me learn LaTeX and solve computer problems, and my thanks also to the physics staff members Audra Xanders, Susan Cantrell, Cindi Raymond, and for their willingness to give help whenever I needed it. Also, I want to thank my wife Jelly and son Paul for their understanding, love, and support. And my mom and dad who always encouraged me and prayed for me.

TABLE OF CONTENTS

LIST OF TABLES

LIST OF FIGURES

Figure Page

Figure Page

CHAPTER I

INTRODUCTION

The Standard Model (SM)

The Standard Model is based on a Lagrangian that contains all observed particles in nature. It is symmetric under poincaré transformations, as any theory must be. But it is also symmetric under internal local symmetry transformations based on the gauge group $U(1)_Y \times SU(2)_W \times SU(3)_C$ where Y, W, and C stand for the hypercharge, weak isospin, and color respectively. The observed fermions are arranged in the following multiplets.

$$\Psi^L = \begin{pmatrix} \nu \\ e \end{pmatrix}_L, \; e_R, \; Q_L = \begin{pmatrix} u_i \\ d_i \end{pmatrix}_L, \; u_{Ri}, \; d_{Ri} \tag{1}$$

where the subscript L and R stand for the left and right-handed particles. The left-handed particles are doublets under $SU(2)_W$, while the right-handed particles are singlets. The index i stand for the $SU(3)_C$ indices. The quarks are triplets under $SU(3)_C$, while the leptons are singlets. Equation (1) shows the first family of fermions. There are two other families. All three are shown in Table I. Their multiplet stucture under $U(1)_Y \times SU(2)_W \times SU(3)_C$ is the same as the first family.

By Noether's theorem we know that symmetry implies conserved quantities. The invariance of a Lagrangian under poincaré transformations results in conservation of energy, momentum and angular momentum. This is a good reason to believe a Lagrangian should be invariant under poincaré transformations. But, what about the local gauge symmetries? All they appear to do at first glance is to mix the fields in the multiplets. Could this have a physical result? The answer, since I've begged

Table I. The SM particle nomenclature

1	2	3
electron neutrino $\equiv \nu_e$	muon neutrino $\equiv \nu_\mu$	tauon neutrino $\equiv \nu_\tau$
electron$\equiv$ e	muon$\equiv \mu$	tauon $\equiv \tau$
up quark$\equiv$ u	charm quark$\equiv$c	top quark $\equiv$t
down quark$\equiv$ d	strange quark$\equiv$ s	bottom quark $\equiv$b

it, is probably obvious. Yes. The result of the symmetry of the Lagrangian under those symmetry operators is conservation of their corresponding charges. And, since electric charge is conserved, that's a good reason to belive that Lagrangians should be symmetric under such groups. Not only that but the SM is invariant under these group transformations even if the corresponding parameters are allowed to be functions of space-time. This is called local gauge invariance. In such a case the charge is conserved at every point in space, that is, in every particle interaction. This is the state of affairs in the SM. The charges conserved in the SM at low energy are the electric charge and color. However, something else is implied by the invariance of the Lagrangian under the local group symmetry. That is the existence of additional particles. Indeed, particles beyond the matter particles do exist in nature, such as the familiar photon. In fact, the SM predicted the existence of several additional particles before they were observed. In the model, it is the demanding of local invariance of the Lagrangian under the group symmetries that requires the introduction of these particles. A theory that is locally invariant like the SM is called a gauge theory; the particle symmetries are called guage symmetries and the particles implied by the symmetries are called gauge particles. The gauge particles are the messenger particles that transmit forces between the matter particles or between the gauge particles themselves. In the SM the gauge symmetries are with respect to the groups $SU(2)_W$, $U(1)_Y$ and $SU(3)_C$. I said the SM implies conservation of electric charge and color. Where did these other charges come from? Well, actually the SM story begins at energies corresponding to temperatures much higher than those at which we live. That is the SM is not only a model that explains the present but

also a theory that explains the past, back maybe as long ago as 10^{-32} seconds after the beginning (big bang). At that time, and that energy ($\sim 10^{14}$ GeV), the SM was invariant under $SU(2)_W \times U(1)_Y$. But, as the universe cooled it underwent a phase transition, a change in state. At an energy scale of 100 GeV, the $U(1)_Y \times SU(2)_W$ symmetry broke down spontaneously to $U(1)_{EM}$. The universe never lost its color symmetry. The question is how does the SM lose the weak and hypercharge symmetries and gain the electric charge symmetry, and what are the implications of such a symmetry transition? Before I try to answer that question let me first introduce you to the rest of the SM.

The SM Lagrangian is

$$L = L_F + L_G + L_S + L_Y \tag{2}$$

where the subscript F indicates the fermion sector of the Lagrangian which contains the kinetic energy terms for the fermions. The subsript G refers to the gauge particle sector. It contains the kinetic energy terms for the gauge particles. The subscript S refers to the kinetic and potential energy terms of a scalar particle, called the Higgs particle. None of these terms contain mass terms because they would destroy the particle gauge symmetries $SU(2)_W$ and $U(1)_Y$. And finally, the Y subscript refers to the sector in the Lagrangian that connects fermion fields to the scalar boson field. It is called the Yukawa term. The explicit form of these terms are given below.

The fermion term is

$$L_F = \bar{\Psi}(i\not{D})\Psi \tag{3}$$

where

$$\not{D} = \gamma^\mu D_\mu. \tag{4}$$

The γ^μ are the Dirac matrices and, for a single local gauge symmetry,

$$D_\mu = \partial_\mu + igT_iA_{\mu i}. \tag{5}$$

The symbol g is the gauge coupling, the T_i are the generators and $A_{\mu i}$ are the gauge fields. For the three group symmetry of the SM, there are three gauge couplings,

denoted by g_1,g_2, and g_3. The gauge fields belong to the adjoint representations of the gauge groups. They transform as

$$A_{i\mu}(x) \rightarrow A_{i\mu}(x) + \partial_\mu \beta_i(x) + igf_{ijk}\beta_j(x)A_{k\mu}(x) \tag{6}$$

where the f_{ijk} are the structure constants of the group

$$[T_i, T_j] = if_{ijk}T_k. \tag{7}$$

Since $U(1)_Y$ has only one generator, $f_{ijk} = 0$ for this group.

The gauge term for the SM is

$$L_G = -\frac{1}{4}B^{\mu\nu}B_{\mu\nu} - \frac{1}{4}W_i^{\mu\nu}W_{i\mu\nu} - \frac{1}{4}G_i^{\mu\nu}G_{i\mu\nu} \tag{8}$$

where μ and ν are summed over and

$$X_i^{\mu\nu} = \partial^\mu X_i^\nu - \partial^\nu X_i^\mu - gf_{ijk}X_j^\mu X_k^\nu \tag{9}$$

The scalar term is

$$L_S = (D^\mu \phi)^\dagger (D_\mu \phi) - V(\phi) \tag{10}$$

where V is the potential energy of the field ϕ, and ϕ is a complex scalar doublet with respect to $SU(2)_W$

$$\Phi = \begin{pmatrix} \phi^+ \\ \phi^0 \end{pmatrix}. \tag{11}$$

This is the SM Higgs doublet. The electric charges for the matter fields are given by $Q = I_3 + \frac{Y}{2}$, where I_3 is the third component of the isospin and Y is the hypercharge. And the Yukawa term is

$$L_Y = -h^e_{\alpha\beta}\bar{e}_{R\alpha}\phi^\dagger \Psi_{L\beta} - h^d_{\alpha\beta}\bar{d}_{R\alpha}\phi^\dagger Q_{L\beta} - h^u_{\alpha\beta}\bar{u}_{R\alpha}\phi_c^\dagger Q_{L\beta} \tag{12}$$

where α and β are family indices and are summed over and $\phi_c = i\sigma_2\phi^*$.

The problem was that Lagrangian symmetries like these don't allow mass terms and hence don't predict massive particles. This was a serious problem because, even before 1967, scientists realized that the particles did indeed have mass. This was the stumbling stone to understanding how to generate the masses of the particles

without destroying gauge symmetry explicitly. If one simply added explicit mass terms to the Lagrangian, the symetry is broken explicitly and, it makes the theory have infinities. This would render the theory meaningless. The problem was solved in 1967 by Weinberg, Salam and Glashow by incorporating spontaneous symmetry breaking. These men built the SM, incorperating earlier work done by other scientists like Higgs and Nambu. And it was proved by a brilliant mathematicion 't Hooft that the theory was in fact finite and renormalizable. Here is the way they did it. Besides constructing the specific symmetry structure and particle assignments described above, they used the Higgs scalar potential energy in the model to obtain a non-zero vacuum expectation value for the scalar field. Here's how. The potential energy of the scalar field is

$$V(\phi) = -\mu^2 \phi^\dagger \phi + \frac{1}{2}\lambda(\phi^\dagger \phi)^2. \tag{13}$$

This function has a minimum, not at zero vacuum expectation value (vev) for ϕ but at

$$|\phi| = \sqrt{\frac{\mu^2}{2\lambda}} \equiv v. \tag{14}$$

This means the universe could have a ground state energy that does not respect the $U(1)_Y \times SU(2)_W$ symmetry. Thus, the Lagrangian respects the symmetry, but the ground state does not. This is called spontaneous symmetry breaking and is similar to the breaking of rotational symmetry by ferromagnets. The result of this non-intuitive idea is that by perturbatively expanding the scalar around the minimum of the potential there is a shift in the field. That is, the field becomes explicitly

$$\phi = \begin{pmatrix} \phi_3 + i\phi_4 \\ \phi_1 + v + i\phi_2 \end{pmatrix} \tag{15}$$

where v is the vacuum expectation value of ψ and the vevs of $\phi_{1,2,3,4}$ are zero and v is a real constant. We can rewrite ϕ as

$$\phi = \exp\left(ig_2\alpha(x)_i T_i^{SU(2)}\right) \begin{pmatrix} 0 \\ \phi + v \end{pmatrix}. \tag{16}$$

This is called the unitary guage. If ϕ is substituted into the above Lagrangian and the Lagrangian is then written in the unitary gauge, the particles that are supposed

to, like the electron and quarks, but not the photon, get massive. The symmetry reduces to the U(1) electric charge symmetry and the color symmetry, which agrees with nature. It also, predicts the massive gauge bosons that were searched for, and discovered as a result. The SM is beautiful. It has 9 massless gauge bosons corresponding to the exact remaining gauge symmetry $U(1)_{EM} \times SU(3)_C$ and three massive gauge bosons: W^+, W^-, Z^0.

The Standard Model is still, well, the standard. To this day there is no iron clad evidence that the standard model is wrong, except perhaps in the area of neutrino physics, which will be discussed shortly. However, by no means have scientists put away their slide rules and begun fretting that all has been discovered. In fact, there are reasons to believe the SM is only approximately true, at low energies. That there could be other heavier particles that can only be produced at higher energies that are not in the SM.

Questions not answered by the Standard Model

In spite of the remarkable agreement between the SM and experiments, the SM fails to answer some very important questions. For example, the range in masses of the fermions goes from $.5MeV$ for the electron to $\sim 174GeV$ for the top quark. Since the same mechanism is responsible for giving masses to all the massive fermions, why such a huge range in their masses? This is the fermion mass hierarchy problem.

I mentioned the SM is a theory that can explain the past in addition to the present. The values of the parameters in the SM depend on the energy scale. Their values at low energy aren't the same as at high energy. When the three SM gauge couplings are evolved from the present energy to higher energy there is an energy at which all three (almost) intersect. If the coupling constants do intersect then there would be a new single group symetry with one charge instead of three. The idea is that this unification symmetry breaks down to the SM when the energy drops below the critical value, just like the SM breaks down to $U(1)_{EM} \times SU(3)_C$ below the electroweak energy scale. This is Grand Unification Theory (GUT). And the energy at which the couplings approximately intersect is the GUT energy. But the problem

with GUTs is that when the mass of the Higgs boson is evolved from the GUT energy to the present energy it is corrected by a term proportional to the GUT energy. The GUT energy is $\sim 10^{16} GeV$. So, there's no good reason why the mass of the Higgs at our low energy shouldn't be much larger than the electroweak scale ($\sim 250 GeV$). But the Higgs mustn't be much larger than the electroweak scale or else it won't be able to participate in contributions to cross sections necessary to cancel contributions that grow too fast with energy. Otherwise, the cross sections would become larger than the observed cross sections. This is the gauge hierarchy problem. Supersymmetry (SUSY) solves this problem by giving every fermion (boson) a bosonic (fermionic) partner with the same mass and couplings. Since fermionic partners contribute to the boson mass correction with the same strength, but with opposite sign as the bosons, the total quadratic correction is then zero, and the hierarchy problem vanishes. There is much activity going on aimed at measuring SUSY particles.

Also, the SM says nothing about particles with spin higher than $s = 1$. Yet there are theories that predict the existence of fundamental particles with higher spin. For example, in supersymmetry there is the gravitino ($s = \frac{3}{2}$) and the graviton ($s = 2$). Some string theories also allow for particles with higher spins and masses far below the Planck mass [1]. It is also possible that new bound states could exist that have higher spin, like a quark-Higgs or quark-gluon bound state. Such a particle would have spin $\frac{3}{2}$ and would be a color triplet like a quark. In fact there might be fundamental spin $\frac{3}{2}$ color triplets. In Chapter 2, I investigate the production and detection of such a particle.

Massive neutrinos

When explaining the SM I mentioned the Yukawa term in the Lagrangian. When the scalar field develops its vacuum expectation value and is shifted it is the Yukawa term which gives mass to the fermions. After the column matrices are multiplied together and terms in v are collected we get mass terms like

$$M^e_{\alpha\beta} \bar{e}_{R\alpha} e_{L\beta} \tag{17}$$

for the leptons, and similar ones for the up and down quarks. Here, $M^e_{\alpha\beta} = h^e_{\alpha\beta}v$. And as usual, α and β are family indices. The matrix $M^e_{\alpha\beta}$ is a mass matrix. Diagonalizing it gives

$$M^e_\alpha \bar{e}_{R\alpha} e_{L\alpha} \tag{18}$$

where α is the only sum index. But looking at only one term, say $\alpha = 1$, we have

$$M^e \bar{e}_R e_L. \tag{19}$$

This is the electron mass term. Notice that it connects left and right-handed fields. This is true of all charged fermion mass terms. But notice that there are no right-handed neutrinos in the SM. Therefore, there is no mechanism within the SM to give them mass. However, there is growing evidence that neutrinos are massive. Therefore, it is important to determine how to extend the SM to give mass to neutrinos. The most obvious way, perhaps, is to simply include right-handed neutrinos N^R_β in the SM. If three right-handed neutrinos (one for each generation) were added we get a Dirac neutrino mass matrix in the Yukawa term of the Lagrangian similar to the one for the charged leptons

$$L_{Dirac} = -M_{\alpha\beta}\bar{N}_{R\alpha}\nu_{L\beta} \tag{20}$$

that would give three massive Dirac neutrinos upon diagonalization. The right-handed particles are invariant (singlets) under the weak, color and hypercharge symmetries. Hence, right-handed neutrinos have no interaction with any bosons or other matter fields. So, right-handed neutrinos are sterile. Since this is so, there can be a sterile mass term

$$L_{sterile} = -\frac{1}{2}A_{\alpha\beta}\bar{N}_{R\alpha}\hat{N}_{L\beta} \tag{21}$$

in addition to the Dirac mass terms. Where the hat on a field means it is the charge-parity (CP) conjugate field. There is nothing to prevent such a mass term in the case of sterile neutrinos since they have no observable charge. These are called Majorana mass terms, and these right-handed neutrinos are called Majorana neutrinos. So there is no constraint from symmetry against adding by hand such terms to the SM

Lagrangian. The Dirac and Majorana mass terms can be combined

$$L_{Dirac+Sterile} = -M_{\alpha\beta}\bar{N}_{R\alpha}\nu_{L\beta} - \frac{1}{2}A_{\alpha\beta}\bar{N}_{R\alpha}\hat{N}_{L\beta} \tag{22}$$

and expressed as a matrix equation

$$L_{mass} = -\frac{1}{2}\begin{pmatrix} \bar{\hat{\nu}}_R & \bar{N^R} \end{pmatrix}\begin{pmatrix} 0 & M^T \\ M & A \end{pmatrix}\begin{pmatrix} \nu_L \\ \hat{N}_L \end{pmatrix} \tag{23}$$

where ν_L and N_R are columns containing the neutrinos from the three generations and M and A are 3×3 matrices and I've used $M_{\beta\alpha}\bar{\hat{\nu}}_{R\beta}\hat{N}_{L\alpha} = M_{\alpha\beta}\bar{N}_{R\alpha}\nu_{L\beta}$. This mass matrix is a Majorana mass matrix because some bilinears connect one particle and one antiparticle of opposite chirality and all mass eigenstates are Majorana neutrinos. Majaorana mass matrices are required to be symmetric, as this one is.

Now we address the question of how to generate very small masses for neutrinos. To simplify matters for the moment let's pretend there is just one generation. So in eqaution (23), ν_L and N_R are are just the neutrino fields and M and A are numbers. So the mass matrix has two eigenvalues. One is negative but the negative sign can be absorbed into the definition of the neutrino field. The eigenvalues are then given by

$$m_{1,2} = \frac{1}{2}(\sqrt{A^2 + 4M^2} \pm A). \tag{24}$$

Since the M element came from the usual SM symmetry breaking we would expect it to be about the same size as the mass of the charged fermion $SU(2)_W$ partner of the neutrino. But the A element has another origin. Recall, it was put in by hand. We could therefore speculate that this mass occurs at a much higher energy scale (maybe the GUT scale), and is much larger in size. If so, the eigenvalues are approximately

$$m_1 = A \quad m_2 = \frac{M^2}{A}. \tag{25}$$

So, one mass eigenstate is very heavy, too heavy to be seen, and one is very light, much lighter than its $SU(2)_W$ charged partner. This would explain the lightness of the neutrino compared to its charged fermion partner. In the actual case of three generations one obtains three ultra-heavy neutrinos and three very light neutrinos

with masses proportional to the masses of their charged fermion partners. This model would then predict a light neutrino hierarchy similar to the hierarchy of the charged partners. This mechanism is called the *see-saw* mechanism.

There are other ways of introducing mass terms into the SM without disturbing its symmetry. One is to introduce a scalar $SU(2)_W$ triplet into the theory:

$$\Delta = \begin{pmatrix} \Delta_0 \\ \Delta_- \\ \Delta_{--} \end{pmatrix}. \tag{26}$$

Then we can write an $SU(2)_W$ singlet

$$L_{singlet} = -f_{\alpha\beta}\bar{\hat{\psi}}_{R\alpha}\tau \cdot \Delta\psi_{L\beta} \tag{27}$$

where the vector components of τ are the 2×2 $SU(2)$ group generators. Since the fermion bilinear is just the symmetric $SU(2)_W$ triplet combination of two doublets, its dot product with the scalar triplet is a singlet. When the scalar triplet develops a vev in the direction of the neutral component, as before, the vacuum expectation of the scalar is

$$< 0|\Delta|0 >= \begin{pmatrix} v' \\ 0 \\ 0 \end{pmatrix}. \tag{28}$$

So $L_{singlet}$ contains a neutrino mass term.

$$L_{mass} = M_{\alpha\beta}\bar{\hat{\nu}}_{R\alpha}\nu_{L\beta} \tag{29}$$

where $M_{\alpha\beta} = f_{\alpha\beta}v'$. This mass matrix can be diagonalized to obtain massive Majorana neutrinos, without violating the SM symmetry. However, this spontaneous symmetry breaking would contribute mass terms for the gauge bosons in the same way the SM symetry breaking did. And could give a different value of the ratio of the gauge boson masses. Therefore, since the ratio predicted by the SM in good agreement with experiment, we must have

$$v' \ll v. \tag{30}$$

Since fermion masses are prportional to vevs, the above requirement is consistent with the neutrinos being much less massive than the other fermions.

We could combine the two methods outlined above for giving mass to the neutrinos. Instead of adding three right-handed neutrinos though, we might only add one. Perhaps the other two are too heavy to be seen. Incidentally, for reasons I'll soon reveal, we don't want this sterile neutrino to be heavy but rather very light. In this case the three active SM neutrinos could mix with the sterile through the regular SM Yukawa Lagrangian, as in the first case above. But the three active neutrinos could mix via a new scalar triplet, as in the second case above. That way we would obtain a 4×4 neutrino mass matrix with three active neutrinos and one sterile. Such a mass matrix could appear as

$$M = \begin{pmatrix} m_{ss} & m_{se} & m_{s\mu} & m_{s\tau} \\ m_{es} & m_{ee} & m_{e\mu} & m_{e\tau} \\ m_{\mu s} & m_{\mu e} & m_{\mu\mu} & m_{\mu\tau} \\ m_{\tau s} & m_{\tau e} & m_{\tau\mu} & m_{\tau\tau} \end{pmatrix} \tag{31}$$

where the 1-1 element comes from the sterile mass term like in the example above. The other members in the top row and first column come from the Yukawa interactions between the right-handed sterile and the active neutrinos. The 3×3 block containing the rest of the elements are from the new scalar triplet that combines the active neutrinos. Since some bilinears connect a particle and antiparticle, this mass matrix is Majorana, and hence must be symmetric.

This mass matrix is the preferred mass matrix experimentally, even if its origen has nothing to with the method by which it was obtained above. In fact, a sterile neutrio doesn't have to be one of the Dirac partners of one of the active neutrinos in the SM. It's origin may have nothing to do with the SM. But regardless of how such a mass matrix occurs, the experimental data currently favors three active neutrinos plus a sterile neutrino. The reason the fourth neutrino must be sterile is because of the constraint from Z-decay at the LEP collider ($Z \to \nu_i \bar{\nu}_i$). The measurement of of the visible width of the and the total width of the Z-boson at the LEP collider

showed that the total number of light $SU(2)_W$ doublet light neutrinos is equal to three (Here, light means $m_\nu < \frac{m_Z}{2}$).

Neutrino oscillations in vacuum

Now if the 4×4 mass matrix in equation (31) is diagonalized the eigenvalues and the unitary matrix that relates the flavor basis and the mass basis can be found. It is neutrino flavor states that interact with matter. But neutrinos propagate according to the time dependent Schröedinger equation, as a superposition of energy eigenstates. This difference of bases is responsible for the possibility that a neutrino produced as a certain flavor will change into some other flavor after propagating some distance. The eigenvectors of the mass matrix are the mass eigenstates.

$$M_D x_m = m x_m. \tag{32}$$

This equation is in the mass basis so the subscript D means the mass matrix is diagonal and the subscript m identifies the mass basis. Since the mass matrix is symmetric, the matrix in the flavor basis is related to the diagonal matrix in the mass basis by a single unitary operator. We have

$$U^T M_f U U^T x_f = m U^T x_f \tag{33}$$

where the subscript f identifies the flavor basis. Comparing these two equations we have

$$U^T x_f = x_m. \tag{34}$$

Or,

$$x_f = U x_m. \tag{35}$$

Therefore,

$$|\nu_\alpha >= U_{\alpha i} |\nu_i > \tag{36}$$

where α is a flavor label and i is a mass eigenstate label. The time dependent relationship between the flavor states and mass eigenstates is

$$|\nu_\alpha(t) >= \exp(-iE_i t) U_{\alpha i} |\nu_i > \tag{37}$$

where $E_i = \sqrt{p^2 + m_i^2}$ is the energy of an eigenstate with momentum p and mass m_i. Now, let us find the probability that a neutrino initially in the flavor state α could be found in the flavor state β sometime later. The probability amplitude is given by

$$< \nu_\beta|\nu_\alpha(t) >=< \nu_\beta| \exp(-iE_it)U_{\alpha i}|\nu_i > \tag{38}$$

$$=< \nu_j|U^\dagger_{j\beta} \exp(-iE_it)U_{\alpha i}|\nu_i > \tag{39}$$

$$= \exp(-iE_it)U_{\alpha i}U^*_{\beta i} \tag{40}$$

where we have summed over j and used the orthonormality of the mass eigenstates. So, the probability of the flavor transition is

$$P(\nu_\alpha \to \nu_\beta) = | < \nu_\beta|\nu_\alpha(t) > |^2 \tag{41}$$

$$= \sum_{i,j}(\exp(-iE_it)U_{\alpha i}U^*_{\beta i})(\exp(-iE_jt)U_{\alpha j}U^*_{\beta j})^* \tag{42}$$

$$= \sum_{i,j} U_{\alpha i}U^*_{\beta i}U^*_{\alpha j}U_{\beta j} \exp(i(E_j - E_i)t). \tag{43}$$

If the unitary matrix is real, we can write the probability

$$P(\nu_\alpha \to \nu_\beta) = \sum_{i,j} U_{\alpha i}U_{\beta i}U_{\alpha j}U_{\beta j} \left(\frac{\exp(i(E_j - E_i)t) + \exp(-i(E_j - E_i)t}{2}\right)$$

$$= \sum_{i,j} U_{\alpha i}U_{\beta i}U_{\alpha j}U_{\beta j} \cos((E_j - E_i)t)$$

$$= \delta_{\alpha\beta} + \sum_{i,j} U_{\alpha i}U_{\beta i}U_{\alpha j}U_{\beta j}(\cos((E_j - E_i)t) - 1) \tag{44}$$

where the dummy indices were interchanged and the probability was added to itself and the sum was divided by two. Also, we've used

$$\sum_{i,j} U_{\alpha i}U_{\beta i}U_{\alpha j}U_{\beta j} = \delta_{\alpha\beta}. \tag{45}$$

The last expression of the probability becomes

$$P(\nu_\alpha \to \nu_\beta) = \delta_{\alpha\beta} + \sum_{i,j} U_{\alpha i}U_{\beta i}U_{\alpha j}U_{\beta j} \left(-2\sin^2\left(\frac{(E_j - E_i)t}{2}\right)\right). \tag{46}$$

This equation is symmetric in the dummy indexes, and terms with $i = j$ are absent. So, we can express the probability in the form

$$P(\nu_\alpha \to \nu_\beta) = \delta_{\alpha\beta} - \sum_{i<j} 4U_{\alpha i}U_{\beta i}U_{\alpha j}U_{\beta j} \sin^2\left(\frac{(E_j - E_i)t}{2}\right). \tag{47}$$

Now, being so light, neutrinos are extremely relativistic $p \gg m_i$ so the energy $E_i = \sqrt{p^2 + m_i^2}$ can be approximated $E_i \simeq p + \frac{m_i^2}{2p}$. Therefore, $E_j - E_i \simeq \frac{m_j^2 - m_i^2}{2p}$, and $t \simeq x$, and as already shown, $p \simeq E$. and the probability becomes

$$P(\nu_\alpha \to \nu_\beta) = \delta_{\alpha\beta} - \sum_{i<j} 4U_{\alpha i}U_{\beta i}U_{\alpha j}U_{\beta j} \sin^2\left(\frac{\delta m_{ji}^2 x}{4E}\right) \tag{48}$$

where $\delta m_{ji}^2 = m_j^2 - m_i^2$. But, so far we've expressed the probability in natural units. Converting over to more convenient units we have

$$P(\nu_\alpha \to \nu_\beta) = \delta_{\alpha\beta} - \sum_{i<j} 4U_{\alpha i}U_{\beta i}U_{\alpha j}U_{\beta j} \sin^2\left(\frac{1.27\delta m_{ji}^2 x}{E}\right) \tag{49}$$

where x is now in kilometers, E is in GeV, and the δm_{ji}^2 are in eV. This could also be written as

$$P(\nu_\alpha \to \nu_\beta) = \delta_{\alpha\beta} - \sum_{i<j} 4U_{\alpha i}U_{\beta i}U_{\alpha j}U_{\beta j} \sin^2\left(\frac{2\pi x}{L_{ji}}\right) \tag{50}$$

if $L_{ji} \equiv \frac{\pi}{1.27\delta m_{ji}^2}$. The quantities L_{ji} are the oscillation lengths associated with the mass-squared-differences δm_{ji}^2. Or (and I promise this is the last form I'll introduce for the probability for now), we could write the probabillity as

$$P(\nu_\alpha \to \nu_\beta) = \delta_{\alpha\beta} - \sum_{i<j} 4U_{\alpha i}U_{\beta i}U_{\alpha j}U_{\beta j} \sin^2(\Delta_{ji}) \tag{51}$$

if $\Delta_{ji} \equiv \frac{2\pi x}{L_{ji}} = \frac{1.27\delta m_{ji}^2 x}{E}$. Now we have expressions for the probability that a neutrino of one flavor will oscillate into another as it propagates through the vacuum. But what about when neutrinos propagate through matter?

Neutrino oscillations in matter

Propagation through matter is not CP invariant because in this case the probabilities do depend on the sign of the δm_{ji}^2 even if the vacuum probabilities don't. In the case of oscillations of neutrinos in the sun we should expect this because neutrinos and antineutrinos don't interact with the sun in the same way. When an electron neutrino travels the sun it undergoes both charged current (the messenger boson is charged) and neutral current (the messenger boson is neutral) elastic collisions with

electrons, whereas when muon or tauon neutrinos propagate, they only experience neutral current elastic interactions since there are very few muons and tauons in the sun. Since interactions modify the effective mass of the electron neutrino differently than the other neutrinos the unitary matrix that relates the flavor and mass eigenstates must compensate, hence the probabilities change. The interactions of antineutrinos are different than for the neutrinos because there aren't many antielectrons, antimuons, and antitauons in the sun. Therefore, the way antineutrinos mix will be different than for neutrinos.

As an example of why these statements are true consider oscillations between only two neutrino flavors ν_e and ν_x in the sun, where x can be μ,τ, or a sterile neutrino s. The unitary matrix in the case of two flavors, in vacuum is

$$U = \begin{pmatrix} \cos(\theta) & -\sin(\theta) \\ \sin(\theta) & \cos(\theta) \end{pmatrix}. \tag{52}$$

The effective hamiltonian in the flavor basis for neutrinos in matter is approximately

$$H^f_{eff} = p + \frac{m_x^2+m_e^2}{4p} + \begin{pmatrix} -\frac{\delta m^2}{4p}\cos(2\theta) + V_{ee} & \frac{\delta m^2}{4p}\sin(2\theta) \\ \frac{\delta m^2}{4p}\sin(2\theta) & \frac{\delta m^2}{4p}\cos(2\theta) + V_{xx} \end{pmatrix} \tag{53}$$

where V_{ee} and V_{xx} are the effective potential energies of the neutrinos due to their interactions with matter and $\delta m^2 = m_x^2 - m_e^2$. The effective mixing angle in matter is given by

$$\tan(2\tilde{\theta}) = \frac{\delta m^2 \sin(2\theta)}{\delta m^2 \cos(2\theta) - 2(V_{ee} - V_{xx})p}. \tag{54}$$

If

$$\delta m^2 \cos(2\theta) - 2(V_{ee} - V_{xx})p = 0 \tag{55}$$

the effective mixing is maximal, even if the vacuum mixing angle is very small. Therefore, the relative sign between δm^2 and $V_{ee} - V_{xx}$ is important. Unless their signs are the same, the effect will suppress rather than enhance oscillations. The sign of the potentials is opposite for antineutrinos. Therefore, if an oscillation is enhanced for neutrinos, it will be suppressed for antineutrinos. This type of oscillation

enhancement/suppression is called MSW after Mikheyev, Smirnov and Wolfenstein [2].

If $x = \mu$ or τ then $V_{ee} = \sqrt{2}G_F n_e + -\frac{G_F n_n}{\sqrt{2}}$ and $V_{xx} = -\frac{G_F n_n}{\sqrt{2}}$. Where n_n is the number density of neutrons in the matter, n_e is the number density of electrons, and G_F is the Fermi constant given above. The $\sqrt{2}G_F n_e$ term comes from the elastic charged current interactions of the electron neutrino with with electrons in the sun, which is absent for the muon or tauon neutrinos since there are few muons and tauons in the sun. The $-\frac{G_F n_n}{\sqrt{2}}$ term came from the neutral current interactions of the neutrinos with the neutrons in the sun. Neutral current interactions with electrons and protons are absent since they have opposite signs and cancel out. Since $V_{ee} > V_{xx}$ in this case, m_x must be larger than m_e in order for enhanced oscillations to occur. If $x = s$ then $V_{ee} = \sqrt{2}G_F n_e + -\frac{G_F n_n}{\sqrt{2}}$ and $V_{xx} = 0$. In this case too, the mass of the electron neutrino must be lighter. In particular if the electron is created in the sun then in order for MSW enhancement to work, the sterile neutrino has to be heavier than the electron neutrino. I have required this in my models.

In the two active flavor case above the probability that the electron produced in the sun would remain an electron neutrino as it left the sun is [3]

$$P(\nu_e \rightarrow \nu_e) = \sin^2(\theta) + P_{LZS}\cos(2\theta) \tag{56}$$

where

$$P_{LZS} = \exp\left(-\frac{\pi \delta m^2 \sin^2(2\theta)}{4E\cos(2\theta)|\frac{d}{dx}\ln(n_e)|res}\right) \tag{57}$$

is the Landau-Zenner-Stuckelberg Probability. The subscript res means that the derivative of the natural log of the electron density is evaluated at the point in the sun where the density passed through the value that temporarily caused maximal mixing between the electron neutrino and the other active neutrino. This formula assumes the electron density to drop off linearly as the electron leaves the sun.

Neutrino experiments

There are three classes of experiments being conducted today that indicate the existence of massive neutrinos. They are the solar experiments [4,5], the atmospheric

experiments [6–8], and the Los Alamos Liquid Scintillator Neutrino Detector (LSND) experiment [9,10].

The MSW mechanism could be important in understanding the solar neutrino experiments. Electron neutrinos are produced in the sun and according to the Standard Solar Model (SSM) [11] we know how many electrons from the sun should be reaching the earth. However, the number of electrons from the sun are about half the SSM prediction. Neutrino oscillations seem the most likely explanation of this discrepancy. If oscillations are the answer two possibilities exist. The supression is due to vacuum oscillations or MSW matter enhanced transitions. If the oscillations are from propagation through the vacuum, the distance between the earth and the sun must correspond to the vacuum oscillation length of the electron neutrino. We can't rule this solution out, even though it would seem highly unlikely that this coincidence would occur. In the case of MSW solutions, there are two possibilities. In one case the vacuum mixing angle between the electron and the neutrino it mixes with is very small. This is called the small angle MSW solar solution. The other case requires a rather large vacuum mixing. This solution is naturally called the large angle MSW solution. It's up to the solar experiments to determine which scenario is correct.

The atmospheric experiments reveal an anomaly. It is based on the ratio of muon neutrinos to electron neutrinos in detectors on the surface of the earth. The atmosphere is continually bombarded by cosmic rays, namely protons. When the protons interact with the atmosphere positive charged pions are produced which quickly decay into a antimuons and muon neutrinos. The antimuons then quickly decay into antimuon neutrinos, electron neutrinos and antielectrons:

$$\pi^+ \rightarrow \mu^+ + \nu_\mu \tag{58}$$

$$\mu^+ \rightarrow \hat{\nu}_\mu + \nu_e + e^+. \tag{59}$$

Simply counting the number of muon neutrinos and electron neutrinos implies that the ratio of muon type neutrinos to electron neutrinos should be about two. However, the experimental results disagree. The measured ratio is about unity. The likely

explanation of this anomaly is that the of the muon neutrinos oscillate into another flavor as they propagate through the vacuum.

The last, but not least, experiment is the LSND experiment at Las Alamos. It measures the appearance of electron type neutrinos in a beam of muon type neutrinos. Two types of experiments were done at LSND and both imply the same δm^2 and mixing amplitude for $\nu_\mu \to \nu_e$ oscillations even though they are quite different in nature. The first experiment done at LSND involved the decay of π^+ that were at rest in a collider beam stop. Protons collided with a target which produced the pions. Most of the pions then come to rest in a beam stop before decaying. When they decay a μ^+ and a muon antineutrino are produced:

$$\pi^+ \to \mu^+ \hat{\nu}_\mu. \tag{60}$$

Then, the reaction

$$\hat{\nu}_e + p \to e^+ + n \tag{61}$$

is looked for in the downstream detector. The number of observed events was 22, with only 4.6 background events. This experiment is the decay at rest (DAR) experiment. A decay in flight (DIF) experiment was also done. Some of the pions produced in the target decay before they get to the beam stop. Therefore, there are ν_μ neutrinos with momentum corresponding to the momentum of the parent pions. Then, electrons with the correct energy are looked for in the downsteam detector. They look for

$$\nu_e + {}^{12}C \to e^- + anything. \tag{62}$$

The number of events was 40, with a background of 22. Both experiments have a length scale of only about 30 meters. In order for the oscillation length of $P(\nu_\mu \to \nu_e)$ to be that small, the corresponding mass-squared-difference must be large compared to the solar and atmospheric experiments. The solar experiment indicates a mass-squared-difference much smaller than either of the other two experiment types. If we accept the best fit values the experiments give for the mass-squared-differences, it seems four neutrinos are needed to explain the LSND results together with the solar and atmospheric neutrino experimental results. Otherwise, it is impossible to get the three mass-squared-differences that are separated by orders of magnitude.

In Chapter 3, I assume the existence of four massive neutrinos for the reason I gave above. One must be sterile, as I've explained. I will analyze 147 mass matrices to see if they can fit the experimental constraints for the small angle MSW, large angle MSW, and vacuum oscillation solutions of the solar discrepancy.

CHAPTER II

SPIN $\frac{3}{2}$ QUARKS

The recent discovery of the top quark at the Fermilab Tevatron, both by the CDF and D0 Collaboration, has filled the last missing ingredient in the fermionic sector of the SM. The measured mass and the cross section values are in agreement with those expected from the Standard Model. With the luminosity and/or energy upgrade of the Tevatron collider and with the commissioning of the LHC, we will be able to explore the missing bosonic ingredient of the SM, namely the Higgs boson. We will also be able to explore the presence of heavy 4th generation fermions and also other exotic gauge bosons and fermions. In this work I consider the production of such an exotic particle, namely a spin $\frac{3}{2}$ quark. Just like an ordinary quark, I assume it to be a color triplet.

It is not outside the realm of possibility that a spin $\frac{3}{2}$ quark could exist as a fundamental particle. We could also have spin $\frac{3}{2}$ bound states of ordinary quarks with gluons or the Higgs boson. There are also theoretical models in which spin $\frac{3}{2}$ quarks arise as bound states of three heavy quarks for sufficiently strong Yukawa couplings [12]. The masses of these bound states are typically expected to be a few TeV. A heavy spin $\frac{3}{2}$ quark could also exist as the lightest Regge recurrences of light spin $\frac{1}{2}$ quarks. These also could exist as Kaluza-Klein modes in string theory if one or more of the compactification radii is of the order of the weak scale rather than the Planck scale. Such weak compactification in the framework of both string theory or field theory has recently become popular [1]. In this work, I consider the collider production of point-like spin $\frac{3}{2}$ color triplet quarks, in pp , $p\bar{p}$ and $\gamma\gamma$ colliders. The production of spin $\frac{3}{2}$ quarks has been previously considered by Moussallam and Soni for hadronic collisions [13]. My analytical results for the gluon fusion subprocess is in disagreement with theirs.

Feynman rules for spin $\frac{3}{2}$ particles

The Lagrangian and the equations of motion for a free spin $\frac{3}{2}$ particle of mass M can be written as [14,15]

$$\mathcal{L} = \bar{\psi}_\alpha \Lambda_{\alpha\beta}\, \psi_\beta \tag{63}$$

$$\Lambda_{\alpha\beta}\, \psi_\beta = 0 \tag{64}$$

where

$$\begin{aligned} \Lambda_{\alpha\beta} &= (i\partial\!\!\!/ - M) g_{\alpha\beta} + iA(\gamma_\alpha \partial_\beta + \gamma_\beta \partial_\alpha) \\ &\quad + \frac{iB}{2} \gamma_\alpha \partial\!\!\!/ \gamma_\beta + CM\, \gamma_\alpha \gamma_\beta \end{aligned} \tag{65}$$

with $B \equiv 3A^2 + 2A + 1$ and $C \equiv 3A^2 + 3A + 1$. The parameter A is arbitrary except that $A \neq -\frac{1}{2}$. The field ψ_α satisfies the subsidiary conditions

$$\gamma_\alpha\, \psi_\alpha = 0 \tag{66}$$

$$\partial_\alpha\, \psi_\alpha = 0\,. \tag{67}$$

The Lagrangian (1) is invariant under the point transformation [15,16]

$$\psi_\alpha \to \psi'_\alpha = \psi_\alpha + d\gamma_\alpha \gamma_\lambda \psi^\lambda \tag{68}$$

$$A \to A' = \frac{A - 2d}{1 + 4d} \tag{69}$$

where d is an arbitrary parameter except $d \neq -\frac{1}{4}$.The propagator $S_{\alpha\beta}(p)$ is given by

$$\begin{aligned} S_{\alpha\beta}(p) &= \frac{1}{p\!\!\!/ - M} \left[g_{\alpha\beta} - \frac{1}{3}\, \gamma_\alpha \gamma_\beta - \frac{2}{3M^2}\, p_\alpha\, p_\beta \right. \\ &\quad \left. - \frac{1}{3M} (\gamma_\alpha p_\beta - \gamma_\beta p_\alpha) \right] \\ &\quad + \left\{ \frac{a^2}{6M^2}\, p\!\!\!/ \gamma_\alpha \gamma_\beta - \frac{ab}{3M}\, \gamma_\alpha \gamma_\beta \right. \\ &\quad \left. + \frac{a}{3M^2}\, \gamma_\alpha\, p_\beta + \frac{ab}{3M^2}\, \gamma_\beta p_\alpha \right\} \end{aligned} \tag{70}$$

where

$$a = \frac{A+1}{2A+1}\ ,\ b \equiv \frac{A}{2A+1}\ .$$

Note that the terms depending on the parameter A disappear on the mass shell. Pascalutsa has proposed that the spin $\frac{3}{2}$ field ψ_α can be redefined so that all the A dependent terms can be absorbed in the definition of ψ_α and no explicit A dependence appears in the propagator [17]. In my calculation, as an additional check, I used the general A dependent propagator given by (70) since the cross sections or any physical quantity is independent of A. Moussallam and Soni took $A = -1$. The interaction Lagrangian for the color triplet spin $\frac{3}{2}$ quarks with the gluons or photon is obtained by using the minimal substitution

$$\partial_\mu \rightarrow D_\mu = \partial_\mu - igA^a_\mu T_a \tag{71}$$

in (63):

$$\mathcal{L}_I = g\bar{\psi}_\alpha \left(\frac{B}{2}\, \gamma^\alpha \gamma^\mu \gamma^\beta + A g^{\alpha\mu} \gamma^\beta + A \gamma^\alpha g^{\mu\beta} + g^{\beta\alpha} \gamma^\mu \right) T_a \psi_\beta A^a_\mu \tag{72}$$

where g is the coupling constant, T_a are group generators and A^a_μ are the gauge fields. In the case of interactions with photons, there is only one generator: the charge operator (Q_e). And there is only one gauge field: the photon, with the electric coupling (e). In the case of interactions with gluons, the T_a are the eight generators of $SU_C(3)$. And there are the eight gluon gauge fields. The coupling is the $SU_C(3)$ strong coupling.

Calculation of cross sections for hadron colliders

In this section, I calculate the cross sections for the processes

$$\bar{p}p \rightarrow Q\bar{Q} + anything \tag{73}$$

and

$$pp \rightarrow Q\bar{Q} + anything \tag{74}$$

where Q represents the spin $\frac{3}{2}$ quark.

The subprocesses contributing to both reactions (73) and (74) are

$$g + g \to Q\bar{Q} \tag{75}$$

and

$$q + \bar{q} \to Q\bar{Q}\,. \tag{76}$$

The Feynman diagrams contributing to the gluon-gluon (gg) and quark-antiquark ($q\bar{q}$) subprocess are shown in figure 1. The amplitudes for the t, u and s-channels are

$$\begin{aligned} M_t \;=\; & g^2 \bar{u}^\rho(p)\left(\gamma^\mu g^{\rho\alpha} + A\gamma^\alpha g^{\mu\rho}\right) T_a \epsilon_{\mu a}(k) \\ & \left\{ \frac{1}{\not p - \not k - M}\left[g^{\alpha\beta} - \frac{1}{3}\gamma^\alpha\gamma^\beta - \frac{2}{3M^2}(p-k)^\alpha (p-k)^\beta \right.\right. \\ & \left. - \frac{1}{3M}\left(\gamma^\alpha (p-k)^\beta - \gamma^\beta (p-k)^\alpha\right)\right] \\ & + \frac{a^2}{6M^2}(\not p - \not k)\gamma^\alpha\gamma^\beta - \frac{ab}{3M}\gamma^\alpha\gamma^\beta \\ & \left. + \frac{a}{3M^2}\gamma^\alpha (p-k)^\beta + \frac{ab}{3M^2}\gamma^\beta (p-k)^\alpha \right\} \\ & \left(\gamma^\nu g^{\beta\sigma} + A\gamma^\beta g^{\sigma\nu}\right) T_b \epsilon_{\nu b}(k') v^\sigma(p') \end{aligned} \tag{77}$$

$$\begin{aligned} M_u \;=\; & g^2 \bar{u}^\rho(p)\left(\gamma^\nu g^{\rho\alpha} + A\gamma^\alpha g^{\nu\rho}\right) T_b \epsilon_{\nu b}(k') \\ & \left\{ \left[g^{\alpha\beta} - \frac{1}{3}\gamma^\alpha\gamma^\beta - \frac{2}{3M^2}(k-p')^\alpha (k-p')^\beta \right.\right. \\ & \left. + \frac{1}{3M}\left(\gamma^\alpha (k-p')^\beta - \gamma^\beta (k-p')^\alpha\right)\right] \frac{1}{\not k - \not p' - M} \\ & + \frac{a^2}{6M^2}(\not k - \not p')\gamma^\alpha\gamma^\beta - \frac{ab}{3M}\gamma^\alpha\gamma^\beta \\ & \left. + \frac{a}{3M^2}\gamma^\alpha (k-p')^\beta + \frac{ab}{3M^2}\gamma^\beta (k-p')^\alpha \right\} \\ & (\gamma^\mu g^{\beta\sigma} + A\gamma^\beta g^{\sigma\mu}) T_a \epsilon_{\mu a}(k) v^\sigma \end{aligned} \tag{78}$$

$$M_s = -g^2 i f_{abc}\,\bar{u}^\rho(p)\gamma^\alpha T_a v^\rho(p')\,\frac{1}{\hat{s}}\,\epsilon_{\mu b}(k)\epsilon_{\nu c}(k') \left[(2k+k')^\nu g^{\mu\alpha} - (k+2k')^\mu g^{\nu\alpha} + (k'-k)^\alpha g^{\mu\nu}\right]. \quad (79)$$

I point out here that although M_t and M_u depend on the contact transformation parameter A, $\sum|M_t^2|$ and $\sum|M_u^2|$, and all the cross terms which are separately independent of A. M_t, M_u and M_s satisfy the appropriate gauge invariance conditions. The amplitude for the quark subprocess (76) is given by

$$M_q = -ig^2\,\frac{1}{\hat{s}}\,\bar{u}^\alpha(p)T_a\gamma^\mu v_\alpha(p')\,\bar{u}(p_1)\gamma_\mu v(p_2)\,. \quad (80)$$

Using (75)–(79), the cross section for the gluon-gluon subprocess is obtained to be [18]

$$\hat{\sigma}(gg\to Q\bar{Q}) = \frac{\pi\alpha_3^2}{116,640\hat{s}}\left\{60\ln\frac{1+\beta}{1-\beta}\left[66y^2+8y +886+5,184\,\frac{1}{y}+1,296\,\frac{1}{y^2}\right] +\beta\left[24y^4+1,178y^3-13,626y^2+11,380y -97,200-602,640\,\frac{1}{y}\right]\right\} \quad (81)$$

where $\alpha_3 \equiv g^2/4\pi$ and $y \equiv \hat{s}/M^2$ and $\beta \equiv \sqrt{1-4/y}$. Most of the coefficients in (81) are in disagreement with those of Eq. (14) of Moussallam and Soni [13]; only the first and last term in the first square bracket and the first term in the second square bracket agree. Professor B. Moussallam has informed me that he has found an algebraic error in their calculations [19]. After correcting for that error, their new results agree with equation (81). For the quark-antiquark subprocess, the cross section is [18]

$$\hat{\sigma}(q\bar{q}\to Q\bar{Q}) = \frac{\pi\alpha_3^2}{81\hat{s}}\,\beta\left[\frac{8}{3}y^2-\frac{16}{3}y-\frac{16}{3}+96\,\frac{1}{y}\right]. \quad (82)$$

This quark-antiquark subprocess was not calculated in [13].

The total cross sections for the processes (73) and (74) are obtained by folding in the appropriate quark, antiquark and gluon momentum distributions. I have used the distributions produced by the CTEQ Collaboration evaluated at $q^2 = M^2$.

In figure 2, I give the contributions to the cross section for spin $\frac{3}{2}$ quark (Q) pair production at the Tevatron ($p\bar{p}$, $\sqrt{s} = 1.8$ TeV) due to the gluon-gluon and quark-antiquark subprocesses and also the total cross section. As expected, at this energy, the cross section is dominated by the quark-antiquark subprocess because, at lower energies, only the quarks have enough energy to participate in heavy quark production. The results for the TeV 2000 ($p\bar{p}$, $\sqrt{s} = 4$ TeV) is shown in figure 3. The quark-antiquark cotribution still dominates.

At LHC (pp, $\sqrt{s} = 14$ TeV), $Q\bar{Q}$ pairs can be copiously produced. The total cross sections, the gluon-gluon contributions and quark-antiquark contributions are shown in figure 4. As expected, at LHC, the cross sections are dominated by the gluon-gluon contributions. This is because, at higher energy, the more numerous gluons are energetic enough to participate in production of the heavy quarks. For $M = 300$ GeV, the total cross section σ is 10^4 pb, while for $M = 1$ TeV, $\sigma = 0.90$ pb. With the projected luminosity [20] of $1.0\times\ 10^{34} cm^{-2}\,\mathrm{sec}^{-1}$, we shall have about 3 billion $Q\bar{Q}$ events for $M = 300$ GeV and about 300,000 for $M = 1$ TeV.

Production in photon-photon collisions

In photon-photon collisons, only the t and u-channel of figure 1 contribute for the $Q\bar{Q}$ pair production. For the cross section, we obtain [18]

$$\begin{aligned}\hat{\sigma}(\gamma\gamma \to Q\bar{Q}) \;=\; & \frac{\pi\alpha^2}{1215\,\hat{s}}\left\{60\ln\frac{1+\beta}{1-\beta}\left[15y^2-8y-22\right.\right.\\ & \left.+648\,\frac{1}{y}-1,296\,\frac{1}{y^2}\right]+\beta\left[3\,y^4+136\,y^3-2,772\,y^2\right.\\ & \left.\left.+6,080\,y-9,720-38,880\,\frac{1}{y}\right]\right\} \qquad (83)\end{aligned}$$

where α is the fine structure constant to be evaluated at $q^2 = M^2$. I gave the spin $\frac{3}{2}$ quarks a charge of $Q_e = 1$ for generality.

The results for the total cross sections for $M = 200$ GeV to 1 TeV are given in figure 5 for $\sqrt{s}$ from 500 GeV to 2.5 TeV.

Detecting spin $\frac{3}{2}$ quarks in colliders

The method to detect spin $\frac{3}{2}$ quarks depends on their nature. I considered three types of spin $\frac{3}{2}$ color triplets. They are: a quark-Higgs bound state, a quark-gluon bound state, and a fundamental spin $\frac{3}{2}$ quark that can undergo weak decay into a top quark and a weak boson. This can occur when the SM is extended to contain the heavy quarks such as in [13]. In all cases below, the SM background will be large and its cross section will wipe out the cross section of the the spin $\frac{3}{2}$ quark. However there are tags that can be used to separate the heavy quark signal from the rest of the QCD background. The tags are isolated leptons in the final state. The leptons produced according to the SM will not be isolated but will be accompanied close by, in angle, a jet. However, in the case of a heavy quark, the isolated leptons are the result of the fact that the heavy quarks produced are moving much slower than the lighter SM quarks. It is the slowness of the heavy quarks that is also responsible for the jets they decay into occupying a broader solid angle and the overall decay products being relatively isotropic. Another tag is the bottom quark vertex detector. It is now possible to directly determine if a decay involves a bottom quark because there is sufficient resolution to see the short bottom track. Since the lifetime of a bottom is known, such a track is tagged. This is also called flavor tagging. Now for the specific cases. First I discuss hadron colliders.

Each quark-Higgs bound state will decay into a quark and a Higgs. The quark with the largest coupling to the Higgs is the top quark, because the Yukawa coupling is proportional to the quark mass. In fact, the top-Higgs coupling might be non-perturbatively large. So, it is not unreasonable that such a bound state is possible. Therefore, the quark that the heavy bound state decays into will be a top quark. The top will decay into a bottom and a weak charged (W^+) boson. The Higgs will decay into two bottom quarks if it is lighter than a weak boson pair. If heavier, it will decay into a weak boson pair. So, each heavy quark gives three bottom quarks and a weak boson or one bottom quark and three weak bosons. Since a heavy quark-antiquark pair is produced there will be six bottom quarks and two weak bosons or

six bosons and two bottom quarks for each heavy pair produced. So, there could be as many as $2 + 12$ jets down to only two jets. In the case of six or more jets the SM background would be strongly supressed by powers of $\alpha_3 = \frac{g_3^2}{4\pi} \sim .1$ and the isotropy of the jets could possibly tag a heavy quark decay. And if the pair decays into six bottoms, the background of such an event would be sufficiently small so that the spin $\frac{3}{2}$ quarks could be seen. But if there were fewer than six jets, there would be at least four charged leptons. It is not easy to get this type event in the SM. This, together with the isolated lepton tag and the isotropic tag should be sufficient to identify the event as a heavy quark decay. I conclude that if quark-Higgs bound states exist, they should be seen at LHC or the upgraded Tevatron.

In the case of quark-gluon bound states, each heavy quark will decay into a quark and a gluon. Therefore each pair of heavy quarks would give four jets. All we have is the isotropic tag. But, this alone won't be enough to identify a heavy quark pair. It might be possible to make such a severe high transverse energy cut that the pair could be identified, since the background drops off very quickly with high transverse energy. That is, demand that a quark pair event have large momentum transverse to the beam direction in order to evade the background, since the SM events will tend to have momentum more in the direction of the beam. It is inconclusive whether the spin $\frac{3}{2}$ could be seen if a quark-gluon bound state.

Finally, I'll discuss the decays of a spin $\frac{3}{2}$ quark that can undergo weak decay into an ordinary top quark and a charged weak boson. Since the top will decay into a bottom quark and charged weak boson, a pair of heavy quarks would give two tops and two charged weak bosons. The tops would each decay into a bottom and a charged weak boson. So, we end up with two bottoms and four charged weak bosons. This would give two bottoms and a maximum of eight other jets, for a total of ten jets. Therefore, once again, there are lots of jets or leptons and so the spin $\frac{3}{2}$ quark events could be sufficiently tagged. The more leptons that show up when all the bosons don't decay into quarks to produce jets, the more neglegible the background becomes, since more α_3 are replaced by α_2 or α. Therefore, if such spin $\frac{3}{2}$ quarks exist, they should be seen at the future hadron colliders.

The fact that no signal at the Tevatron has been observed is probably a good reason to belive that a spin $\frac{3}{2}$ quark would have to weigh more than 200 GeV. The signal for a spin $\frac{3}{2}$ is not the same as the top quark but has several things in common with it. The isotropic tag and isolated leptons should have been noticed, especially since a great effort was being made to find the top quark. Based on the energy of the Tevatron, it is probably safe to say that, if a spin $\frac{3}{2}$ exists, its mass is more than about 300 GeV.

In a photon collider, the QCD background would be drastically reduced and the collider energy wouldn't have to be shared by partons. However, the spin $\frac{3}{2}$ cross section would be reduced too. If the two are reduced by about the same factor, the arguments used for the different types of spin $\frac{3}{2}$ quarks should carry over to photon colliders.

Concluding discussion

I have calculated the production of exotic spin $\frac{3}{2}$ color triplet quarks at high energy hadronic and photon-photon colliders. At LHC, the cross sections are very large and such a particle of mass up to 1 TeV will be copicously produced. At the upgraded Tevatron, the cross sections are somewhat smaller but still could be observable if the mass is 400 GeV or smaller. I have also calculated the production cross sections for photon-photon collisions at various center of mass energies. Finally, I've discussed the method and possiblity of detecting spin $\frac{3}{2}$ at hadron and photon colliders and it appears that if spin $\frac{3}{2}$ quarks exist as quark-Higgs bound states as fundamental particles that experience weak decays, they will be detectable at future colliders.

In writing the interaction (72), I have assumed that the spin $\frac{3}{2}$ quarks are point like. As a result, at very high energy, my cross sections grow like s^3. This will violate tree unitarity for large enough s and so the higher order corrections to the tree diagrams will be important at large s. If there are spin $\frac{3}{2}$ quark bound states, (72) represents an effective interaction, and at very high energy, the cross section

will be damped due to some form factors. As a result, my cross sections would be somewhat over estimated.

CHAPTER III

MASSIVE NEUTRINOS

The experimental status

The long-standing issue of the mass of neutrinos appears to be moving rapidly towards settlement. The improved statistics of the Super-Kamiokande experiment for atmospheric neutrinos – up-down asymmetries of multi-GeV muon neutrinos and of the ratio of ratios of the observed numbers of ν_μ to ν_e to the prediction – bear strong, consistent indications [6] of a non-zero neutrino mass in agreement with the findings of earlier experiments [7,8]. The observed flux of solar neutrinos by all the running experiments – the earlier results from Homestake, Kamiokande, SAGE and GALLEX [4] and the most recent high statistics confirmation of these results by the Super-Kamiokande experiment [5] – is at variance with the theoretical expectations and finds a natural explanation in the framework of oscillation of massive neutrinos [21]. In addition, there is the result from the Los Alamos Liquid Scintillator Neutrino Detector (LSND) which gives the first laboratory evidence for the oscillation of both $\bar{\nu}_\mu \rightarrow \bar{\nu}_e$ [9] as well as $\nu_\mu \rightarrow \nu_e$ type [10]. Based on these experiments there is little doubt that neutrinos have mass, contrary to the SM. Since the experiments indicate neutrino oscillations I analyze 147 neutrino mass matrices to find those that can satisfy all the experimental data and to make predictions, testable in future long-baseline neutrino oscillation experiments.

The need for four neutrinos

In my analyses I assume real mass matrices which give real mixing matrices because I neglect CP violation for vacuum oscillations. Therefore, the probability

for oscillations between flavors α and β may be written

$$P(\nu_\alpha \rightarrow \nu_\beta) = \delta_{\alpha\beta} - 4 \sum_{k<j} U_{\alpha k} U_{\beta k} U_{\alpha j} U_{\beta j} sin^2 \Delta_{jk} \tag{84}$$

where $\Delta_{jk} \equiv \delta m^2_{jk} L/4E = 1.27(\delta m^2_{jk}/eV^2)(L/km)/(GeV/E), \delta m^2_{jk} \equiv m^2_j - m^2_k$. Defining [22] $A^{\alpha\beta}_{jk} \equiv -4U_{\alpha k}U_{\beta k}U_{\alpha j}U_{\beta j}$ the probability is

$$P(\nu_\alpha \rightarrow \nu_\beta) = \delta_{\alpha\beta} + \sum_{k<j} A^{\alpha\beta}_{jk} sin^2 \Delta_{jk}. \tag{85}$$

But, there are only three measured scales for the Δ_{jk}. They correspond to the three mass-squared-difference scales associated with the solar, atmospheric and LSND neutrino experiments. Therefore, the probability is approximately

$$P(\nu_\alpha \rightarrow \nu_\beta) = \delta_{\alpha\beta} + A^{\alpha\beta}_{sun} sin^2 \Delta_{sun} + A^{\alpha\beta}_{atm} sin^2 \Delta_{atm} + A^{\alpha\beta}_{LSND} sin^2 \Delta_{LSND} \tag{86}$$

where Δ_{sun} corresponds to the solar scale, Δ_{atm} to the atmospheric scale and Δ_{LSND} to the LSND scale. The factors $A^{\alpha\beta}_{sun,atm,LSND}$ are the corresponding oscillation amplitudes. The three δm^2 values suggested by the solar, atmospheric, and LSND experiments are vastly different; $\delta m^2 \sim 10^{-5}$ (or10^{-10}), 10^{-3} and 1 eV^2 respectively. With three known neutrinos (ν_e, ν_μ, ν_τ), we can have only two independent δm^2. Thus, a fourth neutrino is required. By the experimental constraints from Z^0 decay at LEP, this fourth neutrino must be sterile (inactive) with respect to the SM. Therefore, one is led to the introduction of a fourth sterile neutrino species which is ultralight (denoted by ν_s) [23,24].

I assume the mass hierachy shown in figure 6. It has been shown that this hierarchy satisfies all the experimental data [24], and also provides a mechanisim whereby neutrinos can contribute to the invisible mass density of the universe.

Flavor scenarios

There are two possible flavor scenarios that can solve the solar and atmospheric experiments. Either the electron neutrinos in the sun oscillate into sterile neutrinos and the atmospheric muon neutrinos oscillate into tau neutrinos or electron neutrinos

in the sun oscillate into tau neutrinos and the atmospheric muon neutrinos oscillate into sterile neutrinos.

Based on the measurements of the ^4He ratio, one might only consider the flavor scenario that $\nu_e \rightarrow \nu_s$ explained the solar puzzle via the small angle MSW oscillation, and $\nu_\mu \rightarrow \nu_\tau$ the atmospheric problem (henceforth, this scenario is designated Scenario A). The reason is that this allows the sterile neutrino mixing with the active neutrinos to be very small. If the cosmological bound on δm^2 and A^{es}_{sun} [25]

$$\delta m^2 A^{es}_{sun} < 10^{-7} eV^2 \tag{87}$$

is correct this is the only possible solution. However, there is some dispute as to what bounds the ^4He ratio implies for the number of neutrino flavors. There are ways of getting around the bound (87). For example, it is possible that oscillations between the active neutrinos and a sterile neutrino can cause asymmetries [26] in the numbers of neutrinos and antineutrinos. This can effect the ^4He ratio in a way that would make a lower value still consistent with four flavors. Therefore, in this analysis I have also considered the second flavor scenario in which the atmospheric problem is solved with large mixing between ν_μ and ν_s and the solar puzzle is explained by oscillations between ν_e and ν_τ. (henceforth, this second scenario is designated Scenario B). The other possibilities, where the atmospheric anomaly is explained by mixing of ν_μ and ν_e are disflavored by the CHOOZ reactor experiment [27] at 90% CL. I don't consider them here.

Experimental constraints

In the paper by Bahcal, Krastev and Smirnov [28] it is pointed out that if a global fit is made to all the data from the chlorine, GALLEX, SAGE and SuperKamiokande (SK) experiments, including the electron neutrino event rates, earth regeneration day-night effect and the preliminary spectral resolution of the electron events at SK, then the large angle MSW solutions to the solar puzzle are ruled out at the 99% CL. Without the spectral resolution they are not. However, I have used the allowed ranges for the solar mass squared differences and solar mixings consistent

Table II. The 95% confidence level ranges for the SAM mass-squared-differences and mixing amplitudes for scenarios A ($x = sterile$) and B ($x = \tau$).

flavor Scenario	mass-squared-difference	A^{ex}_{sun}
$\nu_e \rightarrow \nu_s$	$2.7 \times 10^{-6}\text{eV}^2 - 7 \times 10^{-6}\text{eV}^2$	$3.5 \times 10^{-3} - 1.7 \times 10^{-2}$
$\nu_e \rightarrow \nu_\tau$	$3.5 \times 10^{-6}\text{eV}^2 - 10^{-5}\text{eV}^2$	$3.5 \times 10^{-3} - 1.5 \times 10^{-2}$

with all the data except the spectral resolution results, since the spectral analysis is still preliminary.

The ranges for the neutrino mass-squared-differences and mixing amplitudes [29] that correspond to the small angle MSW [2] (SAM) solutions to the solar neutrino puzzle for both flavor scenarios are shown in Table II.

The ranges in mass squared differences and mixing amplitudes [29] for the large angle MSW (LAM) and vacuum long wavelength (VLW) solutions to the solar puzzle are given in Table III. The solar data allows LAM and VLW solutions with $\nu_e \rightarrow \nu_\tau$ (Scenario B) solar oscillations but the claim has been made that it rules out those with $\nu_e \rightarrow \nu_s$ (Scenario A) at 99% CL [28,29].

The ranges in mass-squared-differences and mixing amplitudes for the allowed by the atmospheric neutrino data [30] is given in Table IV for both flavor scenarios.

Finally, the LSND data [9,10] along with the constraints from the reactor experiment at Bugey [31] and E776 at BNL [32] suggest that

$$..2eV^2 \leq \delta m^2_{e\mu} \leq 3eV^2,\ 2 \times 10^{-3} \leq A^{e\mu}_{LSND} \leq 4 \times 10^{-2} \tag{88}$$

for the electron to muon type oscillations at LSND.

The 4×4 neutrino mass matrices

The most general 4×4 mass matrix has sixteen complex elements. However, since there is no immediate observational necessity of incorporating CP violation in the ν sector, I choose the elements to be real. Further, I assume the mass eigenstates are all Majorana neutrinos. So, the mass matrices are Majorana and are, therefore, symmetric like the one in equation (31).

Table III. The 95% CL ranges for the mass-squared-differences and mixing amplitudes for the LAM and VLW solutions to the solar puzzle.

Oscillation Type	mass-squared-difference	$A^{e\tau}_{sun}$
LAM	$5\times10^{-6}\text{eV}^2 \le \delta m^2 \le 3.6\times10^{-5}\text{eV}^2$	$.4 \le A^{es}_{sun} \le .9$
VLW	$6\times10^{-11}\text{eV}^2 \le \delta m^2 \le 10^{-10}\text{eV}^2$	$.67 \le A^{es}_{sun} \le 1.0$

Consider the mass matrix [33]

$$M = m\begin{pmatrix} \epsilon_1\delta^2 & \epsilon_2\delta^3 & 0 & 0 \\ \epsilon_2\delta^3 & 0 & 0 & \epsilon\delta \\ 0 & 0 & c & s \\ 0 & \epsilon\delta & s & -c \end{pmatrix}. \tag{89}$$

This matrix is written in the basis ν_s (or ν_τ),ν_e,ν_μ,ν_τ (or ν_s). The neutrinos in parentheses refer to scenario B and scenario A is without the parentheses. The powers of delta [22] have been added to fix the hierarchy of the matrix parameters. Such a hierachy is dictated by the experimental data. Delta is a smallness parameter ($\delta \ll 1$). Therefore, the larger the power of the factor of δ on a matrix element, the smaller the element. The relative size of the elements is then made obvious by simple inspection. Also, the factors of δ are handy in computing the approximate eigenvalues and eigenvectors of the matrix. The exact eigenvalues can be expanded in powers of δ. Keeping terms to some power of δ is equivalent to expanding in powers of the matrix paramters and determining what power, for a given parameter, to truncate the expansion by how large it was assumed to be. But, using δ automatically keeps track of the assumed hierachy and allows expansion in only one variable (δ), instead of as many expansions as there are parameters. After the calculations are completed δ is set equal to unity.

The 20 models are obtained by permuting the ϵ_2 and ϵ elements amongst the 1-2, 1-3, 1-4, 2-3, and 2-4 elements in the matrix. The 20 matrices that result are

Table IV. The 95% CL ranges for the atmospheric mass-squared-differences and mixing amplitudes for scenarios A ($x = sterile$) and B ($x = \tau$).

flavor Scenario	mass-squared-difference	A^{ex}_{sun}
$\nu_\mu \to \nu_s$	$8 \times 10^{-4}\text{eV}^2 \leq \delta m^2 \leq 9 \times 10^{-3}\text{eV}^2$	$.75 \leq A^{es}_{sun} \leq 1.0$
$\nu_\mu \to \nu_\tau$	$3.2 \times 10^{-4}\text{eV}^2 \leq \delta m^2 \leq 8 \times 10^{-3}\text{eV}^2$	$.75 \leq A^{es}_{sun} \leq 1.0$

$$M1 = m \begin{pmatrix} \epsilon_1 & \epsilon_2 & 0 & 0 \\ \epsilon_2 & 0 & 0 & \epsilon \\ 0 & 0 & c & s \\ 0 & \epsilon & s & -c \end{pmatrix} \tag{90}$$

$$M2 = m \begin{pmatrix} \epsilon_1 & \epsilon_2 & 0 & 0 \\ \epsilon_2 & 0 & \epsilon & 0 \\ 0 & \epsilon & c & s \\ 0 & 0 & s & -c \end{pmatrix} \tag{91}$$

$$M3 = m \begin{pmatrix} \epsilon_1 & \epsilon_2 & \epsilon & 0 \\ \epsilon_2 & 0 & 0 & 0 \\ \epsilon & 0 & c & s \\ 0 & 0 & s & -c \end{pmatrix} \tag{92}$$

$$M4 = m \begin{pmatrix} \epsilon_1 & \epsilon_2 & 0 & \epsilon \\ \epsilon_2 & 0 & 0 & 0 \\ 0 & 0 & c & s \\ \epsilon & 0 & s & -c \end{pmatrix} \tag{93}$$

$$M5 = m \begin{pmatrix} \epsilon_1 & 0 & \epsilon_2 & 0 \\ 0 & 0 & 0 & \epsilon \\ \epsilon_2 & 0 & c & s \\ 0 & \epsilon & s & -c \end{pmatrix} \tag{94}$$

$$M6 = m \begin{pmatrix} \epsilon_1 & 0 & \epsilon_2 & 0 \\ 0 & 0 & \epsilon & 0 \\ \epsilon_2 & \epsilon & c & s \\ 0 & 0 & s & -c \end{pmatrix} \tag{95}$$

$$M7 = m \begin{pmatrix} \epsilon_1 & 0 & \epsilon_2 & \epsilon \\ 0 & 0 & 0 & 0 \\ \epsilon_2 & 0 & c & s \\ \epsilon & 0 & s & -c \end{pmatrix} \tag{96}$$

$$M8 = m \begin{pmatrix} \epsilon_1 & \epsilon & \epsilon_2 & 0 \\ \epsilon & 0 & 0 & 0 \\ \epsilon_2 & 0 & c & s \\ 0 & 0 & s & -c \end{pmatrix} \tag{97}$$

$$M9 = m \begin{pmatrix} \epsilon_1 & 0 & 0 & \epsilon_2 \\ 0 & 0 & 0 & \epsilon \\ \epsilon_2 & \epsilon & s & -c \end{pmatrix} \tag{98}$$

$$M10 = m \begin{pmatrix} \epsilon_1 & 0 & 0 & \epsilon_2 \\ 0 & 0 & \epsilon & 0 \\ 0 & \epsilon & c & s \\ \epsilon_2 & 0 & s & -c \end{pmatrix} \tag{99}$$

$$M11 = m \begin{pmatrix} \epsilon_1 & 0 & \epsilon & \epsilon_2 \\ 0 & 0 & 0 & 0 \\ \epsilon & 0 & c & s \\ \epsilon_2 & 0 & s & -c \end{pmatrix} \tag{100}$$

$$M12 = m \begin{pmatrix} \epsilon_1 & \epsilon & 0 & \epsilon_2 \\ \epsilon & 0 & 0 & 0 \\ 0 & 0 & c & s \\ \epsilon_2 & 0 & s & -c \end{pmatrix} \tag{101}$$

$$M13 = m \begin{pmatrix} \epsilon_1 & 0 & 0 & 0 \\ 0 & 0 & \epsilon & \epsilon_2 \\ 0 & \epsilon & c & s \\ 0 & \epsilon_2 & s & -c \end{pmatrix} \tag{102}$$

$$M14 = m \begin{pmatrix} \epsilon_1 & \epsilon & 0 & 0 \\ \epsilon & 0 & 0 & \epsilon_2 \\ 0 & 0 & c & s \\ 0 & \epsilon_2 & s & -c \end{pmatrix} \tag{103}$$

$$M15 = m \begin{pmatrix} \epsilon_1 & 0 & \epsilon & 0 \\ 0 & 0 & 0 & \epsilon_2 \\ \epsilon & 0 & c & s \\ 0 & \epsilon_2 & s & -c \end{pmatrix} \tag{104}$$

$$M16 = m \begin{pmatrix} \epsilon_1 & 0 & 0 & \epsilon \\ 0 & 0 & 0 & \epsilon_2 \\ 0 & 0 & c & s \\ \epsilon & \epsilon_2 & s & -c \end{pmatrix} \tag{105}$$

$$M17 = m \begin{pmatrix} \epsilon_1 & 0 & 0 & 0 \\ 0 & 0 & \epsilon_2 & \epsilon \\ 0 & \epsilon_2 & c & s \\ 0 & \epsilon & s & -c \end{pmatrix} \tag{106}$$

Table V. The factors of delta on the five parameters that correspond to the seven hierarchies.

Hierarchy	s	c	ϵ	ϵ_1	ϵ_2
H1	δ^0	δ^0	δ^1	δ^2	δ^3
H2	δ^0	δ^0	δ^1	δ^2	δ^2
H3	δ^0	δ^0	δ^1	δ^3	δ^2
H4	δ^0	δ^1	δ^1	δ^3	δ^3
H5	δ^0	δ^1	δ^1	δ^4	δ^3
H6	δ^0	δ^2	δ^1	δ^3	δ^3
H7	δ^0	δ^2	δ^1	δ^4	δ^3

$$M18 = m \begin{pmatrix} \epsilon_1 & 0 & 0 & \epsilon \\ 0 & 0 & \epsilon_2 & 0 \\ 0 & \epsilon_2 & c & s \\ \epsilon & 0 & s & -c \end{pmatrix} \tag{107}$$

$$M19 = m \begin{pmatrix} \epsilon_1 & 0 & \epsilon & 0 \\ 0 & 0 & \epsilon_2 & 0 \\ \epsilon & \epsilon_2 & c & s \\ 0 & 0 & s & -c \end{pmatrix} \tag{108}$$

$$M20 = m \begin{pmatrix} \epsilon_1 & \epsilon & 0 & 0 \\ \epsilon & 0 & \epsilon_2 & 0 \\ 0 & \epsilon_2 & c & s \\ 0 & 0 & s & -c \end{pmatrix}. \tag{109}$$

For each of the models obtained by permutation I tried seven hierarchies between the matrix parameters. They are shown in Table V.

The 3-4 element in the models isn't far from unity since it controls the large atmospheric mixing angle. The parameters outside the lower right 2×2 sector

of the matrices control the size of the mass-squared-difference that is associated with atmospheric mixing. In particular, I choose ϵ to control the atmospheric mass-squared-difference. So, the size of ϵ relative to the 3-4 element is fixed by experiment. So, in all hierarchies ϵ is multiplied by one power of δ. I call the 2×2 sector containing the elements c,s that control the atmospheric mixing angle the atmospheric sector. The 2×2 sector that contains ϵ_1 and ϵ_2 controls the solar mixing and δm^2. It is, therefore, called the solar sector.

For M1, the hierachies have the following interpretations. In the hierarchy H1 the 1-1 element is much larger than the 1-2 element. This means that the mixing in the solar sector could be small. Therefore, this hierarchy represents a possible SAM solution. Also, the size of the largest element in the solar sector is one order smaller than that of ϵ. This approximately corresponds to the relative size of the measured solar mass-squared-difference to that for atmosphere in a SAM solution. This can be seen if one realizes that since ϵ (multiplied by δ) approximately represents the atmospheric mass splitting, its square (order δ^2) should determine the atmospheric mass-squared-difference. Likewise, it is the largest element in the solar sector (multiplied by δ^2) that determines the solar splitting and its square (order δ^4) that determines the solar mass-squared-difference. This is consistent with the atmospheric $\delta m^2(\sim 10^{-3})$ and the solar $\delta m^2(\sim 10^{-6})$.

In the hierarchy H2 the 1-1 element is the same order as the 1-2 element. This means that the mixing in the solar sector could be large. Therefore, this hierarchy represents a possible LAM or VLM solution. But, the relative size of the solar mass-squared-difference to the atmospheric mass-squared-difference is the same as for H1. So, this hierachy is a possible LAM solution, since in the case of VLW the solar mass-squared-difference is much smaller.

In the hierarchy H3 the 1-1 element is much smaller than the 1-2 element. This means that the mixing in the solar sector could be large. Therefore, this hierarchy represents another possible LAM or VLM solution. But it must be a LAM solution for the same reason H2 must be.

In the hierarchy H4 the 1-1 element is the same order as the 1-2 element. This means that the mixing in the solar sector could be large. Therefore, this hierarchy represents a possible LAM or VLM solution. But, in this case the relative size of the mass squared difference in the solar sector to that of the atmospheric sector is of order δ^4. Given $\delta m^2 \sim 10^{-2}$ for the atmosphere, this would correspond to a $\delta m^2 \sim 10^{-8}$ for the solar. Here, the solar δm^2 is far too small for this to be a LAM solution. Actually, it's too big for this to be a VLW solution. However, the the main function of the δ factors is to maintain hierarchy, not to rigidly commit the parameters to exact relative sizes. Therefore, if we allow some flexibility in the sizes prescribed by the δ factors we can accept this as a possible VLW solution. The same is true about hierarchies H5,H6, and H7.

The above interpretations don't apply to all the 20 models. For example, in the case of M5, the 1-2 element is zero. Hence, even for the H2 and H3 hierarchies it's likely to be a SAM solution. In fact, it turned out that H2 provided a SAM solution, while for H1 and H3 no ranges for the five parameters could be found, which would make the probability variables agree with experiments (i.e. H1 and H3 failed). It could not be forseen that H2 would work, while H1 and H3 would fail. Therefore, it was necessary to try both hierarchies in order to find a solution. Likewise, in the VLW hierarchies I could not be certain that H4, H5, H6, and H7 would fail. Yes, since the 1-2 element is zero we would expect them to fail but it was still possible that the other parameters could cause the large solar mixing needed. For example, although the 1-2 element in M15 is zero, the H7 hierarchy yielded large angle solar mixing. Even so, it failed for other reasons. Therefore, herein I have studied all seven hierachies for each model to find those which work.

A new class of matrices

I also introduce a new matrix that doesn't fit into the same class as the 20 matircies above. This is because the parameter in the 3-3 and 4-4 positions has been moved off the diagonal into the 2-3 position. If these elements are held fixed and the same elements as above were permuted we would obtain 20 more models. However,

here I only treat the seven hierarchies of this single model. It is

$$M21 = m \begin{pmatrix} \epsilon_1 & \epsilon_2 & 0 & 0 \\ \epsilon_2 & 0 & c & \epsilon \\ 0 & c & 0 & 1 \\ 0 & \epsilon & 1 & 0 \end{pmatrix}. \tag{110}$$

Other related mass matrix textures

There have been other discussions of four neutrino mass matrices in the literature. One form [34,35] (which I refer to as M22),

$$M22 = m \begin{pmatrix} \epsilon_1 & \epsilon_2 & 0 & 0 \\ \epsilon_2 & 0 & 0 & \epsilon \\ 0 & 0 & c & s \\ 0 & \epsilon & s & c \end{pmatrix} \tag{111}$$

has been confronted with the data in [35,22]. I have included the seven hierachies for this model in my analysis to check my results with those obtained in [35,22] and so I can compare its predictions with those of my models.

Experimental constraints on model parameters

As indicated in Tables II, III, IV and equation (88), there are three possible solutions to the neutrino anomalies if solar, atmospheric and LSND are all accepted. They are SAM (for either scenario A or B), LAM (for scenario B) and VLW (for scenario B). For each solution there are six experimental constraints. They are the δm^2 measurements and oscillation amplitudes for the sun, atmosphere, and LSND. To obtain these quantities, parameterized in terms of the five parameters in each model I calculated the mass eigenvalues m_1, m_2, m_3, and m_4 and formed the three mass-squared-differences. Since these give the three scales that correspond to the experiments as explained, these quantities give three of the six needed. The other three are obtained by calculating the probabilities in order to get the amplitudes A^{es}_{sun}, $A^{\mu\tau}_{atm}$, and $A^{\mu e}_{LSND}$.

Because of the negative sign on the 4-4 element the matrices M1 thru M20 do not require maximal atmospheric mixing. Therefore, it is convenient to parameterize them in terms of trig functions. That is,

$$c \to \cos(2\gamma) \quad s \to \cos(2\gamma). \tag{112}$$

However, if c is small compared to s, it is simpler to set $s = 1$ and to leave the matrix parameterized in terms of c. Note that the number of parameters is the same in either case. In the case of VLW solutions the size of c must be small compared to s. This is because the parameter c often shows up in the denominator of $A^{e\tau}_{sun}$. If it isn't small enough then we can't achieve $A^{e\tau}_{sun} \sim 1$, which is required for a VLW solution. Also, c shows up in the solar mass-squared-difference (δm^2_{sun}) and if c isn't small enough the difference isn't small enough compared to the other constraints (δm^2_{atm}, $A^{\mu e}_{LSND}$, etc.). Also, for M21 c must be small or it will destroy the correct atmospheric mass-squared-difference. So, maximal mixing is required and $s = 1$. Lastly, without the negative sign on the 4-4 element, M22 [34,35] requires maximal mixing, which implies c is small compared to s. So, $s = 1$ and this model is parameterized in terms of c.

In the analysis I found none of my proposed models M1 thru M21 to be able to fit the VLW experimental constraints. Only M22 [34,35] could do so. In fact, M22 [34,35] was able to fit the SAM, and LAM contraints as well. Of the 21 models that I proposed, M1, M2, M5, M6, M9, M10, and M21 fit the SAM constraints and M1, M2, and M21 fit the LAM constraints. In Tables VI to XX, I show the six constrained quantities in terms of the five parameters of the models for which ranges could be found that caused the six expressions to all fall within the experimental limits. The model, type of solution, and hierarchy that correspond to the parameters are indicated in each table.

Table VI. M1-SAM (H1) parameterization.

Measured Quantity	Parameterization
δm^2_{LSND}	m^2
δm^2_{atm}	$2m^2\epsilon^2\cos(2\gamma)$
δm^2_{sun}	$m^2(\epsilon_1^2 - \epsilon^4\cos^2(2\gamma)$
$A^{\mu e}_{LSND}$	$4\epsilon^2\sin^2(2\gamma)$
$A^{\mu\tau}_{atm}$	$\sin^2(2\gamma)$
A^{es}_{sun}	$(4\epsilon_2^2)/(\epsilon_1 - \epsilon^2\cos(2\gamma))^2$

Table VII. M2-SAM (H1) parameterization.

Measured Quantity	Parameterization
δm^2_{LSND}	m^2
δm^2_{atm}	$2m^2\epsilon^2\cos(2\gamma)$
δm^2_{sun}	$m^2(\epsilon_1^2 - \epsilon^4\cos^2(2\gamma)$
$A^{\mu e}_{LSND}$	$4\epsilon^2\cos^2(2\gamma)$
$A^{\mu\tau}_{atm}$	$\sin^2(2\gamma)$
A^{es}_{sun}	$(4\epsilon_2^2)/(\epsilon_1 + \epsilon^2\cos(2\gamma))^2$

Table VIII. M5-SAM (H2) parameterization.

Measured Quantity	Parameterization
δm^2_{LSND}	m^2
δm^2_{atm}	$2m^2\epsilon^2\cos(2\gamma)$
δm^2_{sun}	$m^2(\epsilon_1^2 - \epsilon^4\cos^2(2\gamma)$
$A^{\mu e}_{LSND}$	$4\epsilon^2\sin^2(2\gamma)$
$A^{\mu\tau}_{atm}$	$\sin^2(2\gamma)$
A^{es}_{sun}	$(4\epsilon^2\epsilon_2^2\sin^2(2\gamma))/(\epsilon_1 - \epsilon^2\cos(2\gamma))^2$

Table IX. M6-SAM (H2) parameterization.

Measured Quantity	Parameterization
δm^2_{LSND}	m^2
δm^2_{atm}	$2m^2\epsilon^2\cos(2\gamma)$
δm^2_{sun}	$m^2(\epsilon_1^2 - \epsilon^4\cos^2(2\gamma)$
$A^{\mu e}_{LSND}$	$4\epsilon^2\cos^2(2\gamma)$
$A^{\mu\tau}_{atm}$	$\sin^2(2\gamma)$
A^{es}_{sun}	$(4\epsilon^2\epsilon_2^2\cos^2(2\gamma))/(\epsilon_1 + \epsilon^2\cos(2\gamma))^2$

Table X. M9-SAM (H2) parameterization.

Measured Quantity	Parameterization
δm^2_{LSND}	m^2
δm^2_{atm}	$2m^2\epsilon^2\cos(2\gamma)$
δm^2_{sun}	$m^2(\epsilon_1^2 - \epsilon^4\cos^2(2\gamma)$
$A^{\mu e}_{LSND}$	$4\epsilon^2\sin^2(2\gamma)$
$A^{\mu\tau}_{atm}$	$\sin^2(2\gamma)$
A^{es}_{sun}	$(4\epsilon^2\epsilon_2^2\cos^2(2\gamma))/(\epsilon_1 - \epsilon^2\cos(2\gamma))^2$

Table XI. M10-SAM (H2) parameterization.

Measured Quantity	Parameterization
δm^2_{LSND}	m^2
δm^2_{atm}	$2m^2\epsilon^2\cos(2\gamma)$
δm^2_{sun}	$m^2(\epsilon_1^2 - \epsilon^4\cos^2(2\gamma)$
$A^{\mu e}_{LSND}$	$4\epsilon^2\cos^2(2\gamma)$
$A^{\mu\tau}_{atm}$	$\sin^2(2\gamma)$
A^{es}_{sun}	$(4\epsilon^2\epsilon_2^2\sin^2(2\gamma))/(\epsilon_1 + \epsilon^2\cos(2\gamma))^2$

Table XII. M21-SAM (H1) parameterization.

Measured Quantity	Parameterization
δm^2_{LSND}	m^2
δm^2_{atm}	$4cm^2\epsilon$
δm^2_{sun}	$m^2(\epsilon_1^2 - 4c^2\epsilon^2)$
$A^{\mu e}_{LSND}$	$4\epsilon^2$
$A^{\mu\tau}_{atm}$	1
A^{es}_{sun}	$(4\epsilon_2^2)/(2c\epsilon + \epsilon_1)^2$

Table XIII. M1-LAM (H2) parameterization.

Measured Quantity	Parameterization
δm^2_{LSND}	m^2
δm^2_{atm}	$2m^2\epsilon^2\cos(2\gamma)$
δm^2_{sun}	$m^2(\epsilon_1 + \epsilon^2\cos(2\gamma))\sqrt{\epsilon_1^2 + 4\epsilon_2^2 - 2\epsilon^2\epsilon_1\cos(2\gamma) + \epsilon^4\cos^2(2\gamma)}$
$A^{\mu e}_{LSND}$	$4\epsilon^2\sin^2(2\gamma)$
$A^{\mu\tau}_{atm}$	$\sin^2(2\gamma)$
A^{es}_{sun}	$(4\epsilon_2^2)/(\epsilon_1^2 + 4\epsilon_2^2 - 2\epsilon^2\epsilon_1\cos(2\gamma) + \epsilon^4\cos^2(2\gamma))$

Table XIV. M2-LAM (H2) parameterization.

Measured Quantity	Parameterization
δm^2_{LSND}	m^2
δm^2_{atm}	$2m^2\epsilon^2\cos(2\gamma)$
δm^2_{sun}	$m^2(\epsilon_1 - \epsilon^2\cos(2\gamma))\sqrt{\epsilon_1^2 + 4\epsilon_2^2 + 2\epsilon^2\epsilon_1\cos(2\gamma) + \epsilon^4\cos^2(2\gamma)}$
$A^{\mu e}_{LSND}$	$4\epsilon^2\cos^2(2\gamma)$
$A^{\mu\tau}_{atm}$	$\sin^2(2\gamma)$
A^{es}_{sun}	$(4\epsilon_2^2)/(\epsilon_1^2 + 4\epsilon_2^2 + 2\epsilon^2\epsilon_1\cos(2\gamma) + \epsilon^4\cos^2(2\gamma))$

Table XV. M21-LAM (H2) parameterization.

Measured Quantity	Parameterization
δm^2_{LSND}	m^2
δm^2_{atm}	$4cm^2\epsilon$
δm^2_{sun}	$m^2(\epsilon_1 - 2c\epsilon)\sqrt{4c^2\epsilon^2 + 4c\epsilon\epsilon_1 + \epsilon_1^2 + 4\epsilon_2^2}$
$A^{\mu e}_{LSND}$	$4\epsilon^2$
$A^{\mu\tau}_{atm}$	1
A^{es}_{sun}	$(4\epsilon_2^2)/(4c^2\epsilon^2 + 4c\epsilon\epsilon_1 + \epsilon_1^2 + 4\epsilon_2^2)$

Table XVI. M22-SAM (H1) parameterization.

Measured Quantity	Parameterization
δm^2_{LSND}	m^2
δm^2_{atm}	$4cm^2$
δm^2_{sun}	$m^2\epsilon_1^2$
$A^{\mu e}_{LSND}$	$4\epsilon^2$
$A^{\mu\tau}_{atm}$	1
A^{es}_{sun}	$(4\epsilon_2^2)/\epsilon_1^2$

Table XVII. M22-LAM (H2) parameterization.

Measured Quantity	Parameterization
δm^2_{LSND}	m^2
δm^2_{atm}	$4cm^2$
δm^2_{sun}	$m^2\epsilon_1\sqrt{\epsilon_1^2 + 4\epsilon_2^2}$
$A^{\mu e}_{LSND}$	$4\epsilon^2$
$A^{\mu\tau}_{atm}$	1
A^{es}_{sun}	$(4\epsilon_2^2)/(\epsilon_1^2 + 4\epsilon_2^2)$

Table XVIII. M22-LAM (H3) parameterization.

Measured Quantity	Parameterization
δm^2_{LSND}	m^2
δm^2_{atm}	$4cm^2$
δm^2_{sun}	$2m^2\epsilon_1\epsilon_2$
$A^{\mu e}_{LSND}$	$4\epsilon^2$
$A^{\mu\tau}_{atm}$	1
A^{es}_{sun}	1

Table XIX. M22-VLW (H6) parameterization.

Measured Quantity	Parameterization
δm^2_{LSND}	m^2
δm^2_{atm}	$4cm^2$
δm^2_{sun}	$m^2\epsilon_1\sqrt{\epsilon_1^2+4\epsilon_2^2}$
$A^{\mu e}_{LSND}$	$4\epsilon^2$
$A^{\mu\tau}_{atm}$	1
A^{es}_{sun}	$(4\epsilon_2^2)/(\epsilon_1^2+4\epsilon_2^2)$

Table XX. M22-VLW (H7) parameterization.

Measured Quantity	Parameterization
δm^2_{LSND}	m^2
δm^2_{atm}	$4cm^2$
δm^2_{sun}	$2m^2(\epsilon_1+c\epsilon^2)\epsilon_2$
$A^{\mu e}_{LSND}$	$4\epsilon^2$
$A^{\mu\tau}_{atm}$	1
A^{es}_{sun}	1

Model parameter ranges

I haven't specified the basis in which the matrices are represented because, until now it hasn't mattered. As mentioned above, the SAM data allows scenarios A and B. But LAM and VLW data only allow scenario B. It is convenient to use different bases when discussing these two scenarios. In the case of scenario A, the basis $\nu_s,\nu_e,\nu_\mu,\nu_\tau$ is the matrix representation that corresponds to the definitions of the solar and atmospheric sectors above. Whereas, in scenario B it is the basis $\nu_\tau,\nu_e,\nu_\mu,\nu_s$. The only difference being that the ν_s and ν_τ flavors are interchanged. And so, when I speak of solutions in scenario A or B, the corresponding basis will apply. If I discuss a LAM or VLW solution it is automatic that the basis is that of B. But if discussing a SAM solution I will distinguish between the bases by putting either an A or B after the name of the matrix to indicate scenario A or B.

A random number generator was used to find the ranges in the parameters that allowed the quantities in Tables VI through XX to satisfy the experimental constraints. The ranges of the parameters that result are shown in Tables XXI through XLII. The parameter γ is defined in equation (112).

Table XXI. M1A-SAM (H1) parameter ranges.

Parameter	Ranges
$m(eV)$	$.45 - 1.74$
γ	$.52 - .76$
ϵ	$2.6 \times 10^{-2} - .1$
ϵ_1	$1.1 \times 10^{-3} - 6.3 \times 10^{-3}$
ϵ_2	$1.5 \times 10^{-5} - 2.1 \times 10^{-4}$

Table XXII. M2A-SAM (H1) parameter ranges.

Parameter	Ranges
$m(eV)$	$.45 - 1.6$
γ	$.52 - .67$
ϵ	$4.7 \times 10^{-2} - .1$
ϵ_1	$1.6 \times 10^{-3} - 6.9 \times 10^{-3}$
ϵ_2	$8.5 \times 10^{-5} - 6.0 \times 10^{-4}$

Table XXIII. M5A-SAM (H2) parameter ranges.

Parameter	Ranges
$m(eV)$	$.45 - 1.75$
γ	$.52 - .77$
ϵ	$2.5 \times 10^{-2} - .1$
ϵ_1	$1.1 \times 10^{-3} - 6.1 \times 10^{-3}$
ϵ_2	$2.3 \times 10^{-4} - 4.4 \times 10^{-3}$

Table XXIV. M6A-SAM (H2) parameter ranges.

Parameter	Ranges
$m(eV)$	$.45 - 1.73$
γ	$.52 - .66$
ϵ	$4.6 \times 10^{-2} - .1$
ϵ_1	$1.6 \times 10^{-3} - 6.7 \times 10^{-3}$
ϵ_2	$4.3 \times 10^{-3} - 10^{-2}$

Table XXV. M9A-SAM (H2) parameter ranges.

Parameter	Ranges
$m(eV)$	$.45 - 1.75$
γ	$.52 - .77$
ϵ	$2.4 \times 10^{-2} - .1$
ϵ_1	$10^{-3} - 7.3 \times 10^{-3}$
ϵ_2	$5.7 \times 10^{-4} - 10^{-2}$

Table XXVI. M10A-SAM (H2) parameter ranges.

Parameter	Ranges
$m(eV)$	$.45 - 1.63$
γ	$.52 - .67$
ϵ	$4.6 \times 10^{-2} - .1$
ϵ_1	$1.6 \times 10^{-3} - 7.0 \times 10^{-3}$
ϵ_2	$2.0 \times 10^{-3} - 8.5 \times 10^{-3}$

Table XXVII. M21A-SAM (H1) parameter ranges.

Parameter	Ranges
$m(eV)$	$.45 - 1.59$
c	$.01 - .1$
ϵ	$2.3 \times 10^{-2} - .1$
ϵ_1	$1.4 \times 10^{-3} - 10^{-2}$
ϵ_2	$8.2 \times 10^{-5} - 1.2 \times 10^{-3}$

Table XXVIII. M1B-SAM (H1) parameter ranges.

Parameter	Ranges
$m(eV)$	$.45 - 1.74$
γ	$.52 - .78$
ϵ	$2.5 \times 10^{-2} - .1$
ϵ_1	$1.1 \times 10^{-3} - 7.8 \times 10^{-3}$
ϵ_2	$1.7 \times 10^{-5} - 3.3 \times 10^{-4}$

Table XXIX. M2B-SAM (H1) parameter ranges.

Parameter	Ranges
$m(eV)$	$.45 - 1.5$
γ	$.52 - .67$
ϵ	$4.7 \times 10^{-2} - .1$
ϵ_1	$2.0 \times 10^{-3} - 7.7 \times 10^{-3}$
ϵ_2	$1.2 \times 10^{-4} - 6.6 \times 10^{-4}$

Table XXX. M5B-SAM (H2) parameter ranges.

Parameter	Ranges
$m(eV)$	$.45 - 1.74$
γ	$.52 - .78$
ϵ	$2.3 \times 10^{-2} - .1$
ϵ_1	$1.2 \times 10^{-3} - 7.9 \times 10^{-3}$
ϵ_2	$3.4 \times 10^{-4} - 8.8 \times 10^{-3}$

Table XXXI. M6B-SAM (H2) parameter ranges.

Parameter	Ranges
$m(eV)$	$.45 - 1.74$
γ	$.52 - .67$
ϵ	$4.6 \times 10^{-2} - .1$
ϵ_1	$1.8 \times 10^{-3} - 8.0 \times 10^{-3}$
ϵ_2	$4.0 \times 10^{-3} - 10^{-2}$

Table XXXII. M9B-SAM (H2) parameter ranges.

Parameter	Ranges
$m(eV)$	$.45 - 1.75$
γ	$.53 - .76$
ϵ	$2.3 \times 10^{-2} - .1$
ϵ_1	$1.2 \times 10^{-3} - 7.8 \times 10^{-3}$
ϵ_2	$7.6 \times 10^{-4} - 10^{-2}$

Table XXXIII. M10B-SAM (H2) parameter ranges.

Parameter	Ranges
$m(eV)$	$.45 - 1.68$
γ	$.52 - .67$
ϵ	$4.7 \times 10^{-2} - .1$
ϵ_1	$1.8 \times 10^{-3} - 8.2 \times 10^{-3}$
ϵ_2	$1.8 \times 10^{-3} - 10^{-2}$

Table XXXIV. M21B-SAM (H1) parameter ranges.

Parameter	Ranges
$m(eV)$	$.45 - 1.74$
c	$.01 - .1$
ϵ	$2.2 \times 10^{-2} - .1$
ϵ_1	$1.9 \times 10^{-3} - 10^{-2}$
ϵ_2	$1.2 \times 10^{-4} - 1.1 \times 10^{-3}$

Table XXXV. M1-LAM (H2) parameter ranges.

Parameter	Ranges
$m(eV)$	$.45 - 1.75$
γ	$.52 - .78$
ϵ	$2.3 \times 10^{-2} - .1$
ϵ_1	$4.7 \times 10^{-6} - 10^{-3}$
ϵ_2	$2.9 \times 10^{-4} - 10^{-2}$

Table XXXVI. M2-LAM (H2) parameter ranges.

Parameter	Ranges
$m(eV)$	$.45 - 1.71$
γ	$.52 - .67$
ϵ	$4.5 \times 10^{-2} - .1$
ϵ_1	$1.7 \times 10^{-3} - 10^{-2}$
ϵ_2	$1.7 \times 10^{-3} - 10^{-2}$

Table XXXVII. M21-LAM (H2) parameter ranges.

Parameter	Ranges
$m(eV)$	$.45 - 1.73$
c	$.01 - .1$
ϵ	$2.2 \times 10^{-2} - .1$
ϵ_1	$1.4 \times 10^{-3} - 10^{-2}$
ϵ_2	$1.2 \times 10^{-3} - 10^{-2}$

Table XXXVIII. M22A-SAM (H1) parameter ranges.

Parameter	Ranges
$m(eV)$	$.45 - 1.49$
c	$1.3 \times 10^{-4} - 10^{-2}$
ϵ	$2.2 \times 10^{-2} - .1$
ϵ_1	$1.3 \times 10^{-3} - 5.6 \times 10^{-3}$
ϵ_2	$5.4 \times 10^{-5} - 3.2 \times 10^{-4}$

Table XXXIX. M22B-SAM (H1) parameter ranges.

Parameter	Ranges
$m(eV)$	$.45 - 1.58$
c	$6.2 \times 10^{-5} - 10^{-2}$
ϵ	$2.3 \times 10^{-2} - .1$
ϵ_1	$1.5 \times 10^{-3} - 6.8 \times 10^{-3}$
ϵ_2	$6.0 \times 10^{-5} - 3.9 \times 10^{-4}$

Table XL. M22-LAM (H2) parameter ranges.

Parameter	Ranges
$m(eV)$	$.45 - 1.74$
c	$3.4 \times 10^{-5} - 10^{-2}$
ϵ	$2.2 \times 10^{-2} - .1$
ϵ_1	$9.6 \times 10^{-4} - 10^{-2}$
ϵ_2	$6.8 \times 10^{-4} - 10^{-2}$

Table XLI. M22-VLW (H6) parameter ranges.

Parameter	Ranges
$m(eV)$	$.45 - 1.74$
c	$5.7 \times 10^{-5} - 10^{-2}$
ϵ	$2.2 \times 10^{-2} - .1$
ϵ_1	$1.8 \times 10^{-7} - 1.5 \times 10^{-5}$
ϵ_2	$3.9 \times 10^{-6} - 10^{-4}$

Suggested experimental tests

Here I briefly discuss some experiments that have been suggested that could possibly test the models.

A muon storage ring has been suggested [36] as a possible source of a neutrino beam resulting from the decay of antimuons into $\bar{\nu_\mu}$ and ν_e. The oscillation of the electron neutrinos into either tau or muon neutrinos could be measured at a detector located some distance away. An example of such an experiment was given [36] in which a storage ring at Fermilab consists of antimuons with an average energy of 20 GeV. One detector could be set up at the Gran Sasso lab in Italy, 10,000 km from Fermilab. Another could be much closer like the SOUDAN mine in Minnesota (740 km). I also suggest that a detector could be set up even closer, say at 10 km. The oscillations these detectors could look for are $\nu_e \rightarrow \nu_\tau$ and $\nu_e \rightarrow \nu_\mu$. The sensitivities in δm^2 and the corresponding mixing angles that they would be capable of are shown in figures 7 thru 22. The Gran Sasso and SOUDAN sensitivities are based on one event per year, while the 10 km sensitivity is based on 100 events per year.

Probability predictions

Once the ranges of the parameters are known it is straightforward to calculate the amplitudes that correspond to different mass-squared-differences for any oscillation and to predict the ranges of their values. I have done so for the oscillation channels that could be measured in the experiments mentioned above. There are

Table XLII. M22-VLW (H7) parameter ranges.

Parameter	Ranges
$m(eV)$	$.45 - 1.75$
c	$5.3 \times 10^{-5} - 10^{-2}$
ϵ	$2.2 \times 10^{-2} - .1$
ϵ_1	$1.1 \times 10^{-8} - 10^{-4}$
ϵ_2	$1.5 \times 10^{-7} - 10^{-4}$

Table XLIII. Parameterized probability amplitudes for $P(\nu_e \rightarrow \nu_\tau)$.

Model-Hierachy	LSND Amplitude	Atmospheric Amplitude
M1A-SAM (H1)	$4\epsilon^2 \cos^2(2\gamma)$	$\epsilon^2 \sin^2(2\gamma)$
M2A-SAM (H1)	$4\epsilon^2 \sin^2(2\gamma)$	$-\epsilon^2 \sin^2(2\gamma)$
M5A-SAM (H2)	$4\epsilon^2 \cos^2(2\gamma)$	$\epsilon^2 \sin^2(2\gamma)$
M6A-SAM (H2)	$4\epsilon^2 \sin^2(2\gamma)$	$-\epsilon^2 \sin^2(2\gamma)$
M9A-SAM (H2)	$4\epsilon^2 \cos^2(2\gamma)$	$\epsilon^2 \sin^2(2\gamma)$
M10A-SAM (H2)	$4\epsilon^2 \sin^2(2\gamma)$	$-\epsilon^2 \sin^2(2\gamma)$
M21A-SAM (H1)	$4c^2$	$\epsilon^2 - c^2$
M22A-SAM (H1)	0.0	ϵ^2

two mass scales that play a role in these experiments. They are the LSND scale and the atmospheric scale of equation (86). The solar mass scale oscillation term is zero since its oscillation wavelength is much larger than these experimental dimensions. The amplitudes of these two oscillation terms in equation (86) will be called the LSND amplitude and the atmospheric amplitude respectively. I show them both in parameterized form for all matrices and hierarchies that were successful in Table XLIII and Table XLIV. Table XLIII shows the amplitudes for $\mathrm{P}(\nu_e \rightarrow \nu_\tau)$ and Table XLIV shows the amplitudes for $\mathrm{P}(\nu_e \rightarrow \nu_\mu)$.

Note the negative signs on some of the terms don't affect the analysis. Incidently, they don't imply the probability is negative since the terms in the probability interfere so that the probability always stays positive. It is like a short Fourier series that represents a positive function.

In Table XLV, I give the predicted probability amplitude ranges of equation (86) for the oscillations at the LSND mass scale and the atmospheric mass scale in the case of $\nu_e \rightarrow \nu_\tau$ oscillations. These are the amplitudes that could be measured in the muon source experiments mentioned above. If only one number is given, it represents both upper and lower limits.

In Table XLVI, I show the probability amplitudes predicted by the models for oscillations of ν_e into ν_μ. Of course, the amplitude at the LSND mass scale is already

Table XLIV. Parameterized probability amplitudes for $P(\nu_e \rightarrow \nu_\mu)$.

Model-Hierachy	LSND Amplitude	Atmospheric Amplitude
M1A,B (H1)	$4\epsilon^2 \sin^2(2\gamma)$	$-\epsilon^2 \sin^2(2\gamma)$
M1B (H2)	$4\epsilon^2 \sin^2(2\gamma)$	$-\epsilon^2 \sin^2(2\gamma)$
M2A,B (H1)	$4\epsilon^2 \cos^2(2\gamma)$	$\epsilon^2 \sin^2(2\gamma)$
M2B (H2)	$4\epsilon^2 \cos^2(2\gamma)$	$\epsilon^2 \sin^2(2\gamma)$
M5A,B (H2)	$4\epsilon^2 \sin^2(2\gamma)$	$-\epsilon^2 \sin^2(2\gamma)$
M6A,B (H2)	$4\epsilon^2 \cos^2(2\gamma)$	$\epsilon^2 \sin^2(2\gamma)$
M9A,B (H2)	$4\epsilon^2 \sin^2(2\gamma)$	$-\epsilon^2 \sin^2(2\gamma)$
M10A,B (H2)	$4\epsilon^2 \cos^2(2\gamma)$	$\epsilon^2 \sin^2(2\gamma)$
M21A,B (H1)	$4\epsilon^2$	$-\epsilon^2 + c^2$
M21B (H2)	$4\epsilon^2$	$-\epsilon^2 + c^2$
M22A,B (H1)	$4\epsilon^2$	$-\epsilon^2$
M22B (H2)	$4\epsilon^2$	$-\epsilon^2$
M22B (H6)	$4\epsilon^2$	$-\epsilon^2$
M22B (H7)	$4\epsilon^2$	$-\epsilon^2$

given above as the LSND experimental costraint. And the predicted amplitudes at this mass scale should be equal to the experimental limits. In fact, they are not the same in all models. In some cases predicted the ranges in these amplitudes are only a subset of the allowed ranges and, therefore, if certain regions of the allowed space are ruled out then some of the models could be disflavored. Only the matrix names are shown because the results were the same regardless of flavor scenario and type of solar solution (SAM, LAM, VLW) or hierarchy.

I also superimposed the ranges in Tables XLV and XLVI onto figures 7 thru 22 that show the sensitivities of the experiments. The rectangular regions indicate the predicted ranges in δm^2 and the corresponding predicted ranges in the amplitudes. Also, in figures 7 thru 22 the range of mixing angles allowed by LSND is indicated by brackets. By placing the predictions on the sesitivity plots of the experiments it can

Table XLV. Predicted amplitudes for $P(\nu_e \rightarrow \nu_\tau)$ oscillations.

Model	LSND Channel	Atm. Channel
M1A-SAM	$4.9 \times 10^{-5} - 7.3 \times 10^{-3}$	$5.5 \times 10^{-4} - 9.6 \times 10^{-3}$
M2A-SAM	$6.7 \times 10^{-3} - 3.8 \times 10^{-2}$	$1.7 \times 10^{-3} - 9.4 \times 10^{-3}$
M5A-SAM	$2.1 \times 10^{-5} - 8.1 \times 10^{-3}$	$5.0 \times 10^{-4} - 9.5 \times 10^{-3}$
M6A-SAM	$6.4 \times 10^{-3} - 3.7 \times 10^{-2}$	$1.6 \times 10^{-3} - 9.3 \times 10^{-3}$
M9A-SAM	$3.5 \times 10^{-5} - 9.2 \times 10^{-3}$	$5.1 \times 10^{-4} - 9.7 \times 10^{-3}$
M10A-SAM	$6.4 \times 10^{-3} - 7.3 \times 10^{-2}$	$1.6 \times 10^{-3} - 9.4 \times 10^{-3}$
M21A-SAM	$4.1 \times 10^{-4} - 4.0 \times 10^{-2}$	$0 - 10^{-2}$
M22A-SAM	0.0	$5.0 \times 10^{-4} - 10^{-2}$

be seen how testable the predictions are, and by indicating the LSND allowed region it is easy to see which predictions are only subsets of the LSND allowed region.

Results

First of all, M22 was the only model to accomodate the VLW constraints. Therefore, if VLW is determined to be the source of the suppression of solar electron neutrinos, my models could be ruled out.

The M22 [35] does not predict an amplitude at the LSND scale in $\nu_e \rightarrow \nu_\tau$ oscillations, whereas all of my models do. Therefore, if these oscillations are measured, M22 [35] would be ruled out. Also, since only scenario A predicts such oscillations if they occur then scenario B can be ruled out. These LSND scale amplitudes are mostly covered by the Fermilab to SOUDAN and the Fimilab to Gran Sasso examples but in some cases the ten kilometer experiment could be useful to cover the entire predicted ranges. The amplitudes at the atmospheric scales are mostly covered by the detector at SOUDAN except for M21, whose minimum predited amplitude is zero. For the $\nu_e \rightarrow \nu_\mu$ oscillations, the complete allowed ranges for the LSND experiment are covered by the detector at SOUDAN and, therefore, so are the predictions. As mentioned above, most of the space allowed by LSND is not predicted by some

Table XLVI. Predicted amplitudes for $P(\nu_\mu \to \nu_e)$ oscillations.

Model	LSND Channel	Atm. Channel
M1	$2.2 \times 10^{-3} - 3.8 \times 10^{-2}$	$5.4 \times 10^{-4} - 10^{-2}$
M2	$2.0 \times 10^{-3} - 9.0 \times 10^{-3}$	$1.7 \times 10^{-3} - 9.3 \times 10^{-3}$
M5	$2.0 \times 10^{-3} - 3.8 \times 10^{-2}$	$5.0 \times 10^{-4} - 9.4 \times 10^{-3}$
M6	$2.0 \times 10^{-3} - 9.1 \times 10^{-3}$	$1.6 \times 10^{-3} - 9.3 \times 10^{-3}$
M9	$2.0 \times 10^{-3} - 3.9 \times 10^{-2}$	$5.1 \times 10^{-4} - 9.6 \times 10^{-3}$
M10	$2.0 \times 10^{-3} - 9.3 \times 10^{-3}$	$1.6 \times 10^{-3} - 9.4 \times 10^{-3}$
M21	$2.0 \times 10^{-3} - 4.0 \times 10^{-2}$	$0.0 - 9.0 \times 10^{-3}$
M22	$2.0 \times 10^{-3} - 4.0 \times 10^{-2}$	$5.0 \times 10^{-4} - 10^{-2}$

of my models in the $\nu_e \to \nu_\mu$ oscillations, whereas the M22 [35] prediction fills the whole LSND allowed region. So, if the small lower end of the allowed mixing angle in the LSND allowed region is ruled out some of my models could be disfavored.

Other experimental tests

Turning now to other tests of the models, the first well known point to emphasize is that the $\nu_e \to \nu_s$ oscillation solution to the solar neutrino problem will be tested once the Sudbury Neutrino Observatory (SNO) measures the neutral current effects of the solar neutrinos. In the $\nu_e \to \nu_\tau$ oscillation scenario one would expect $\Phi_{CC}/\Phi_{NC} \simeq .4$. Where the subscripts CC and NC stand for charged current and neutral current respectively. And Φ represents the signal for the appropriate process before the incorporation of the cross sections and detection efficiencies. This is because both ν_e and ν_τ would interact with the detector via NC interactions, but only ν_e could interact via CC interactions because tauons are too heavy to be produced by solar neutrinos. However, for the $\nu_e \to \nu_s$ case, one should get $\Phi_{CC}/\Phi_{NC} \simeq 1$. This is because only electron neutrinos could interact with the detector via CC or NC interactions because ν_s is sterile.

In the models, the neutrinoless double beta decay vanishes at the tree level since its amplitude is proportional to $< m_{\nu_e} >$ which is given by

$$< m_{\nu_e} >=< \nu_e|M|\nu_e >= M_{\nu_e\nu_e}. \tag{113}$$

Here $M_{\nu_e\nu_e}$ is the $\nu_e - \nu_e$ element of the neutrino mass matrix in the weak basis. Clearly all models predict zero neutrinoless beta decay since this entry vanishes in all models.

Concluding discussion

In this chapter I analyzed 20 mass matrices. For each one, seven matrix element hierarchies were investigated. These hierarchies correspond to different solutions to the solar puzzle: small angle MSW, large angle MSW, and vacuum oscillation. In this group of 140 models, only 8 were found that could satisfy the experimental constraints. Six agreed with the small angle MSW constriants and 2 with the large angle MSW constraints. None of the models could fit the vacuum oscillation constraints. For these 8 models, predictions were made that can be tested in future experiments. Also, I looked at a member of a new class of mass matrices, in the seven hierarchies. Two of the seven models fit the constraints, one to the small and one to the large angle MSW constraints. But, like the other 140 models, none were able to satisfy the vacuum oscillation constraints. I made predictions for the two successful models.

In conclusion, I have found ten four neutrino mass matrices out of 147 models that fit all neutrino observations with five parameters. I have made predictions and shown how they can be tested. I also, mention some measurable differences between my models and that of M22 [35,22].

BIBLIOGRAPHY

1. I. Antoniadis, Phys. Lett. **246B**, 377 (1990); I. Antoniadis, K. Benakali and M. Quiros, Phys. Lett. **331B**, 313 (1994); J. D. Lykken, Phys. Rev. **D54**, 3693 (1996); I. Antoniadis, S. Dimopoulos and G. Dvali, Nucl. Phys. **B516**, 70 (1998); K. R. Dienes, E. Dudas and T. Gherghetta, hep-ph/9803466; N. Arkani-Hamed, S. Dimopoulos and G. Dvali, hep-ph/9803315; A. Pomerol and M. Quiros, hep-ph/9806263.

2. L. Wolfenstein, Phys. Rev. **D17** (1978) 2369; S. P. Mikheyev and A. Smirnov, Yad. Fiz. **42** (1985) 1441; Nuovo Cimento, **9C** (1986) 17.

3. W. C. Haxton, Phys. Rev. Lett., **57** (1986) 1271; S. J. Parks, Phys. Rev. Lett., **57** (1986) 1275.

4. B. T. Cleveland et al. Nucl. Phys. B (Proc. Suppl.) **38** (1995) 47; K. S. Hirata et al., Phys. Rev. **D44** (1991) 2241; GALLEX Collaboration, Phys. Lett. **B388** (1996) 384; J. N. Abdurashitov et al., Phys. Rev. Lett. **77** (1996) 4708.

5. Y. Suzuki, Invited talk at Erice Neutrino workshop, September 17-22, 1997.

6. Y. Fukuda et al., (The Super-Kamiokande collaboration), hep-ex/9807003; T. Kajita, Talk at ν98.

7. K.S. Hirata et al., Phys. Lett. **B280** (1992) 146; R. Becker-Szendy et al., Phys. Rev. **D46** (1992) 3720; W. W. M. Allison et al., Phys. Lett. **B391** (1997) 491.

8. Y. Fukuda et al., Phys. Lett. **B335** (1994) 237.

9. C. Athanassopoulos et al., Phys. Rev. Lett. **75** (1995) 2650; C. Athanassopoulos et al., Phys. Rev. Lett. **77** (1996) 3082.

10. C. Athanassopoulos et al., nucl-ex/9706006; C. Athanassopoulos et al., Phys. Rev. Lett. **81** (1998) 1774.

11. J. N. Bahcall and M. H. Pinsonneault, Rev. Mod. Phys. **67**, 781 (1995).

12. J.G. Taylor, Phys. Lett., **88B**, 291 (1979), and references therein; J.G. Taylor, Phys. Lett., **90B** (1979) 143, and references therein.

13. B. Moussallam and V. Soni, Phys. Rev. **D39** (1988) 1883.

14. W. Rarita and J. Schwinger, Phys. Rev. **60** (1941) 61.

15. P.A. Moldauer and K.M. Case, Phys. Rev. **102** (1956) 279; S.C. Bhargava and H. Watanabe, Nucl. Phys. **87** (1966) 273.

16. L.M. Nath, B. Etemadi and J.D. Kimel, Phys. Rev. **D3** (1970) 2153.

17. V. Pascalutsa, hep-ph/9412321, HU-94-21.

18. Duane A. Dicus, S. C. Gibbons, S. Nandi, hep-ph/9806312.

19. B. Moussallam, Private Communication. I thank Professor Moussallam for helping me to resolve this discrepancy.

20. Review of Particle Physics, Phys. Rev. **D54** (1996) 131.

21. J. Bahcall, *Proceedings of Neutrino'96* edited by K. Enquist, K. Huitu and J. Maalampi (World Scientific, Singapore); A. Smirnov, in Warsaw 1996, ICHEP 96, Vol. 1 p288 (hep-ph/9611465).

22. V. Barger,S. Pakvasa, T. Weiler and K. Whisnant, hep-ph/9806328.

23. D. O. Caldwell and R. N. Mohapatra, Phys. Rev. **D48** (1993) 3259; J. Peltoniemi and J. W. F. Valle, Nucl. Phys. **B406** (1993) 409.

24. S. Goswami, Phys. Rev. **D55** (1997) 2931; S. M. Bilenky, C. Giunti and W. Grimus, Eur. Phys. J. **C1** (1998) 247.

25. R. Barbieri and A. Dolgov, Phys. Lett. **B237** (1990) 440.

26. N.F. Bell, R. Foot, and R.R. Volkas, hep-ph/9805259.

27. CHOOZ Collaboration, M. Apollonio *et al.*, Phys. Lett. **B420** (1998) 397.

28. J.N Bahcall, P.I. Krastev, and A. Yu. Smirnov, Phys. Rev. **D58**:096016 (1998).

29. P. T. Petcov, hep-ph/9806466.

30. M. C. Gonzalez-Garcia, hep-ph/9811407.

31. B. Achkar et al., Nucl. Phys. **B434** (1995) 503.

32. L. Borodovsky et al., Phys. Rev. Lett. **68** (1992) 274.

33. S. C. Gibbons, R. N. Mohapatra, S. Nandi, A. Raychaudhuri, Phys. Lett. **B430** (1998) 296.

34. R. N. Mohapatra, hep-ph/9711444.

35. V. Barger, T. Weiler and K. Whisnant, hep-ph/9712495.

36. S. Geer, hep-ph/9712290.

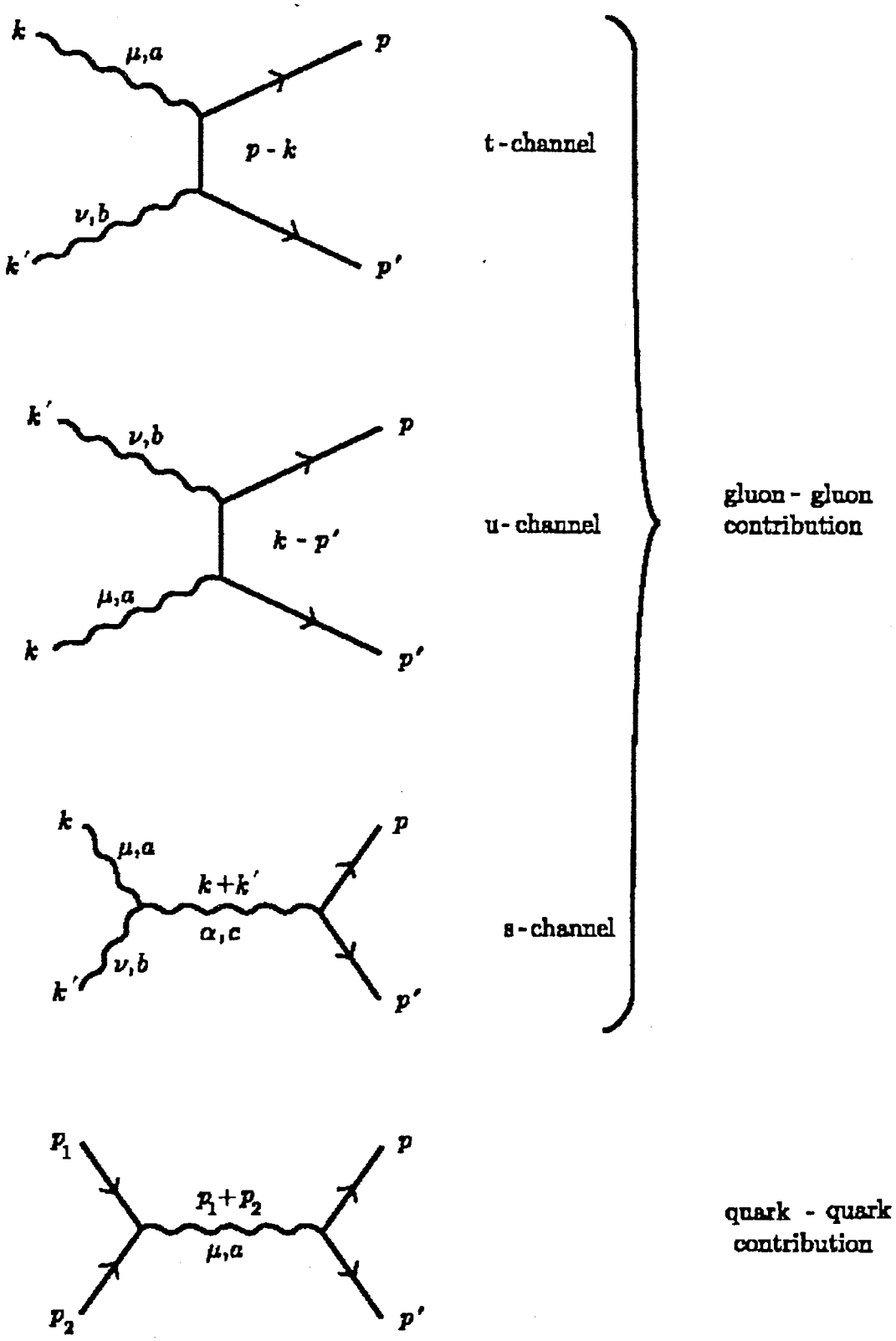

Figure 1: Feynman diagrams for spin 3/2 quark pair production subprocesses.

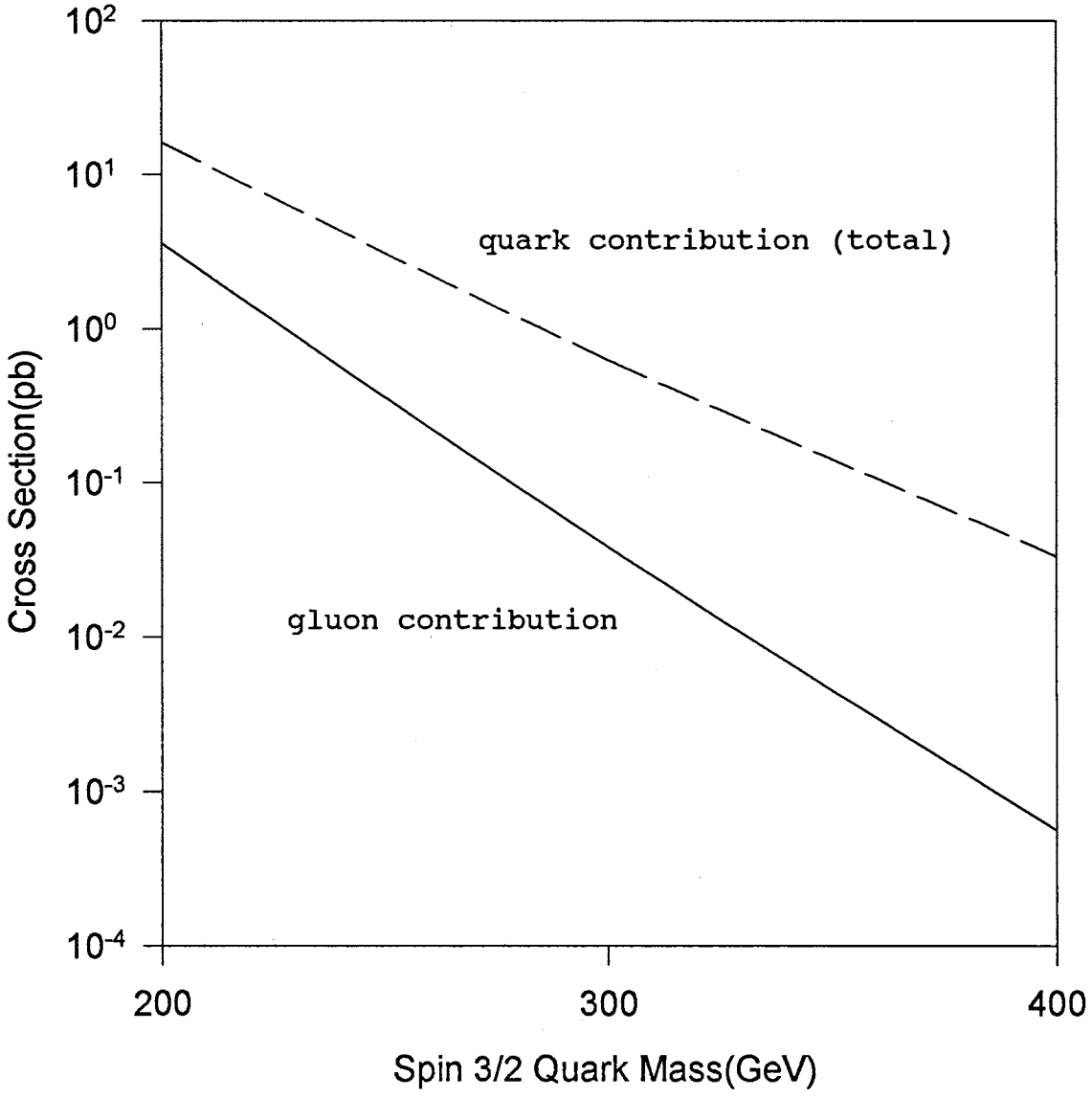

Figure 2: Production of spin 3/2 quarks at the Tevatron.

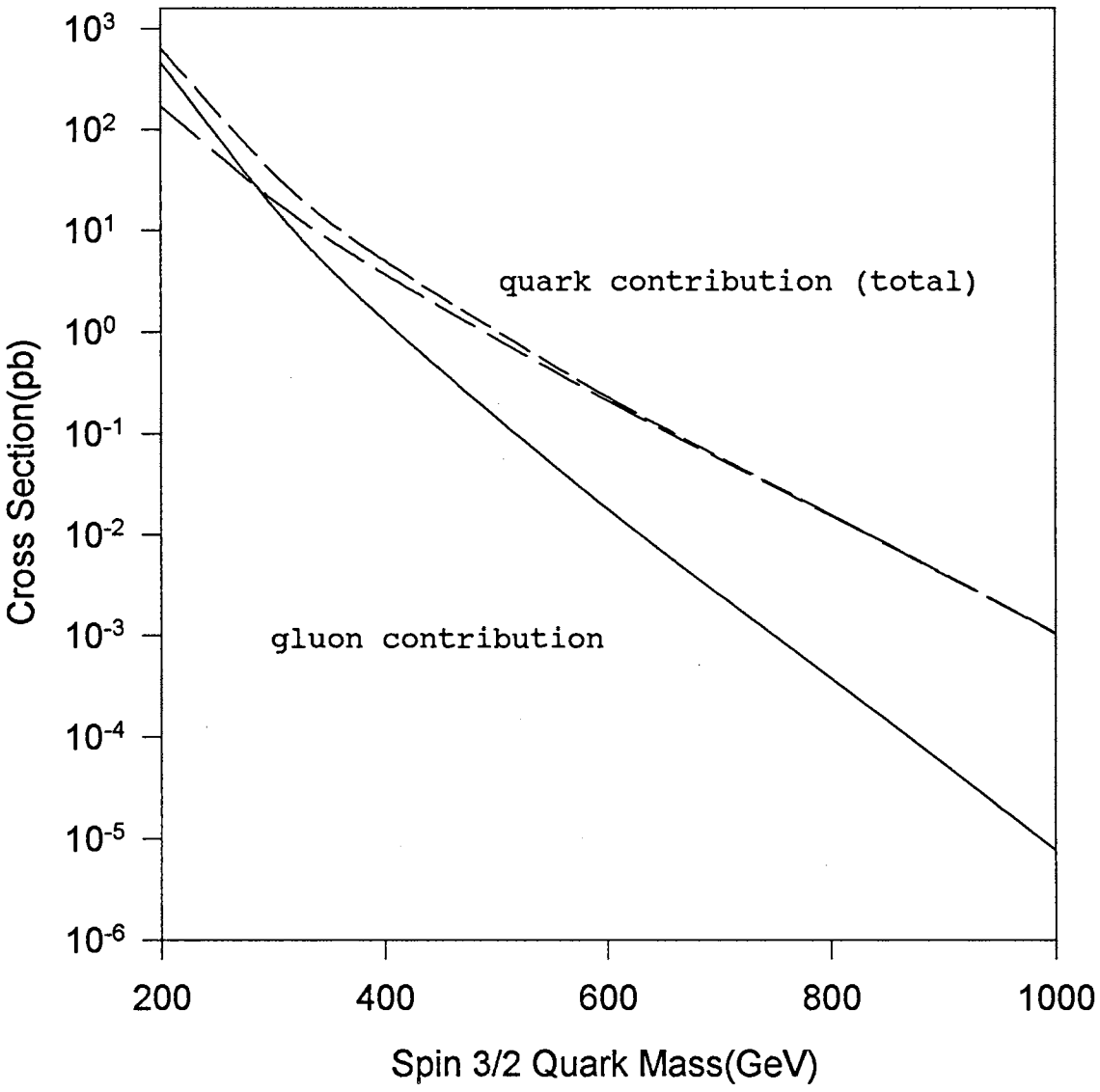

Figure 3: Production of spin 3/2 quarks at Tev 2000.

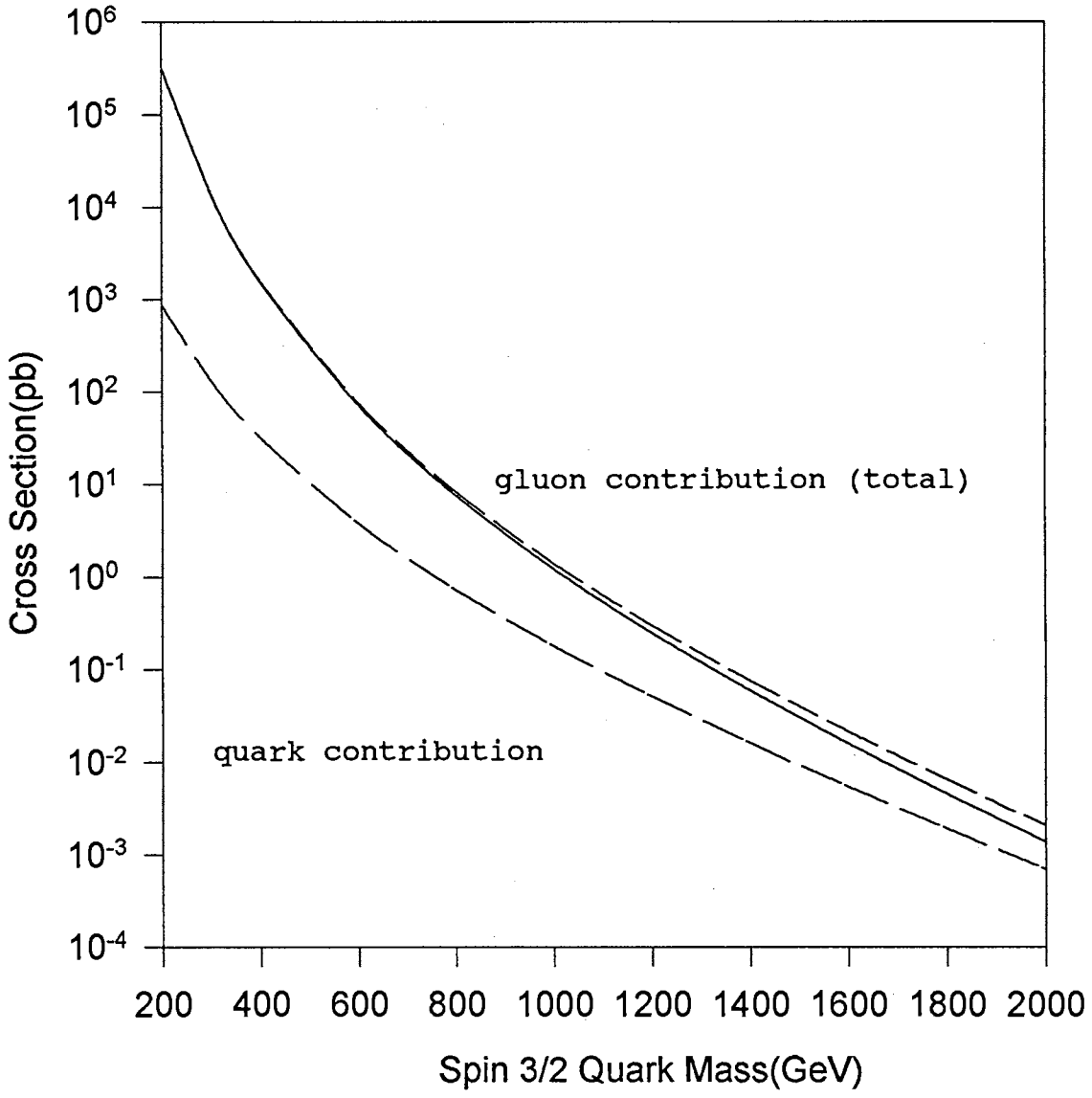

Figure 4: Production of spin 3/2 quarks at LHC.

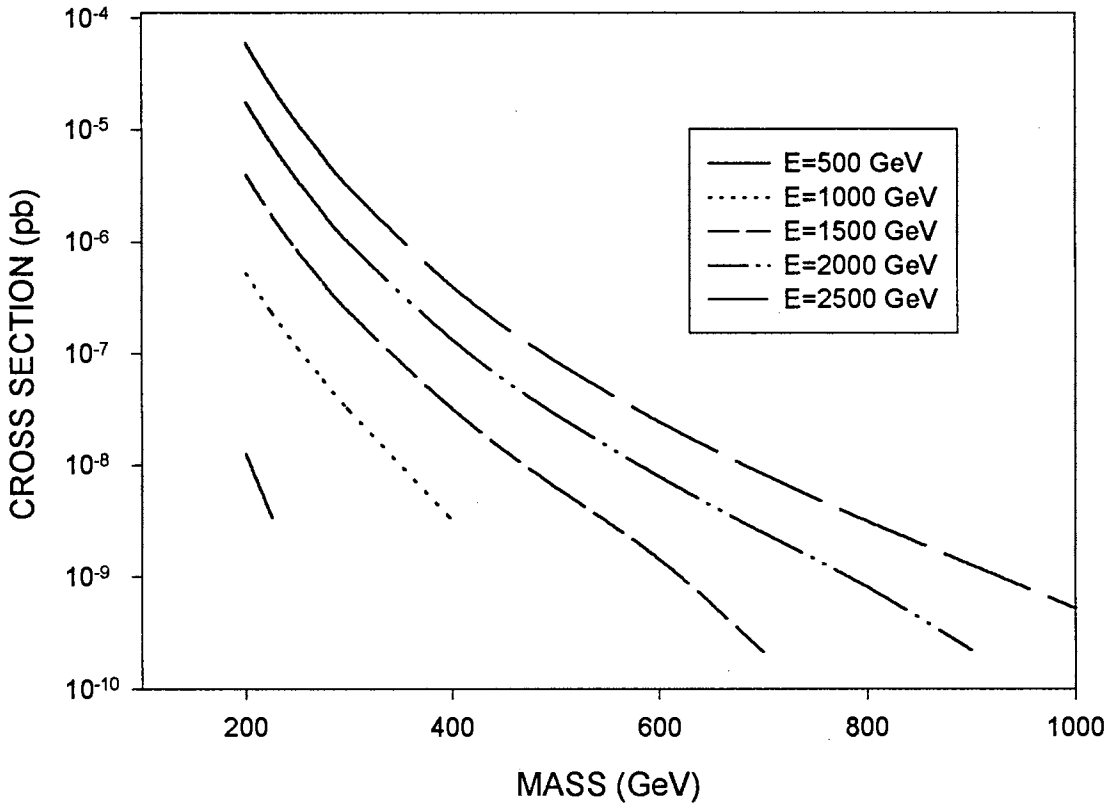

FIG 5: Production of spin 3/2 quarks in photon colliders at various energies

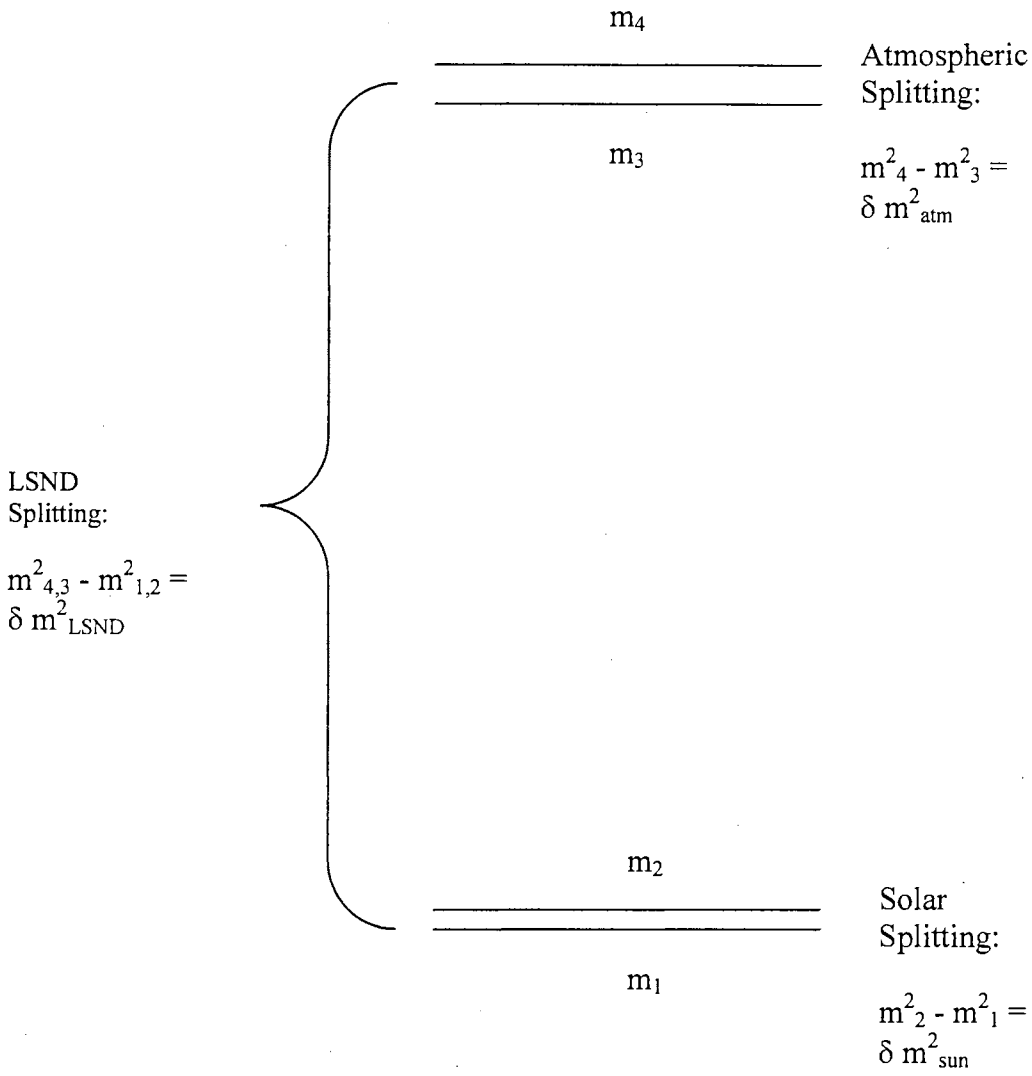

Figure 6: Neutrino mass hierarchy.

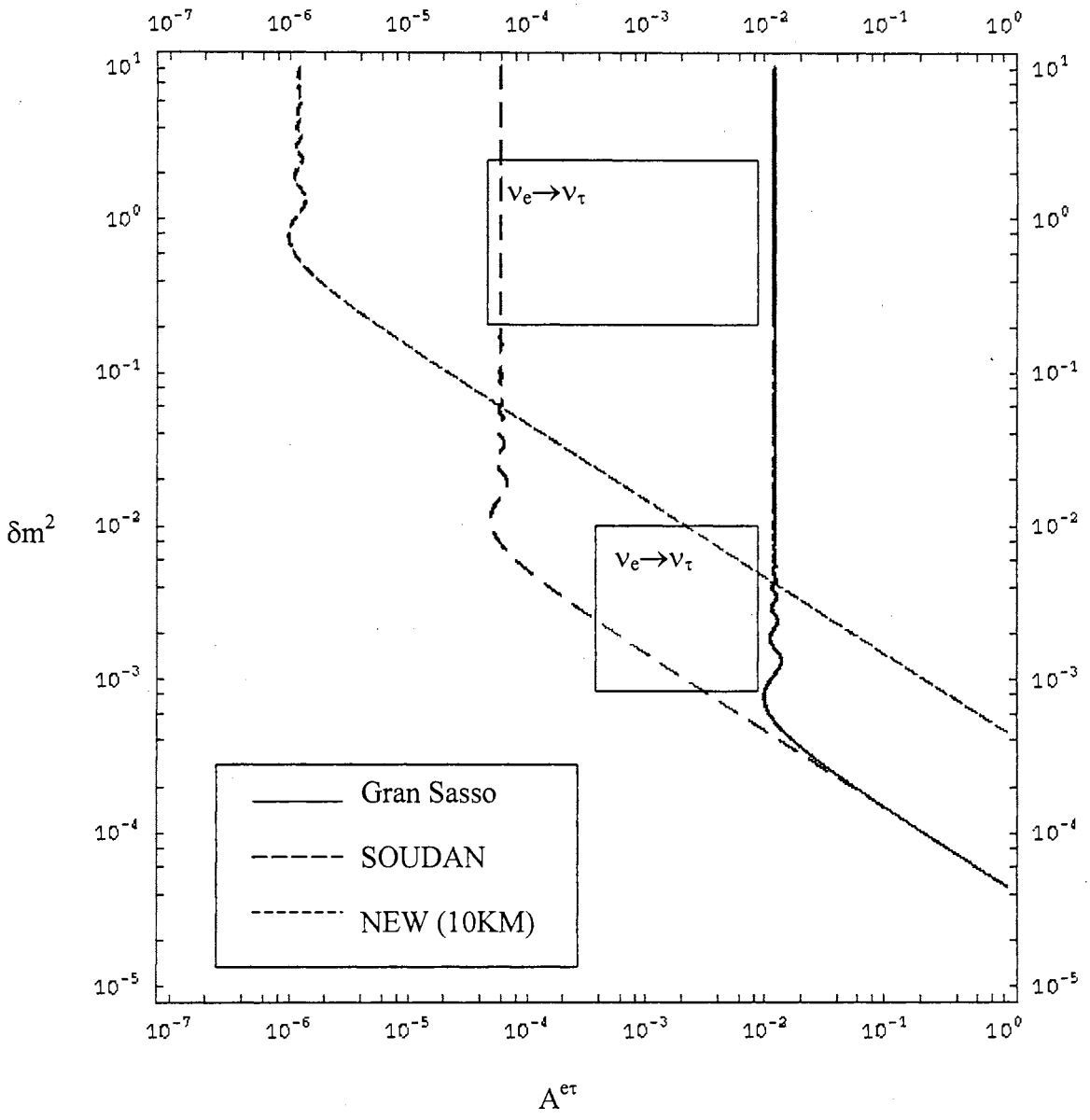

Figure 7. The $\nu_e \rightarrow \nu_\tau$ predicted parameter space for the M1A-SAM model.

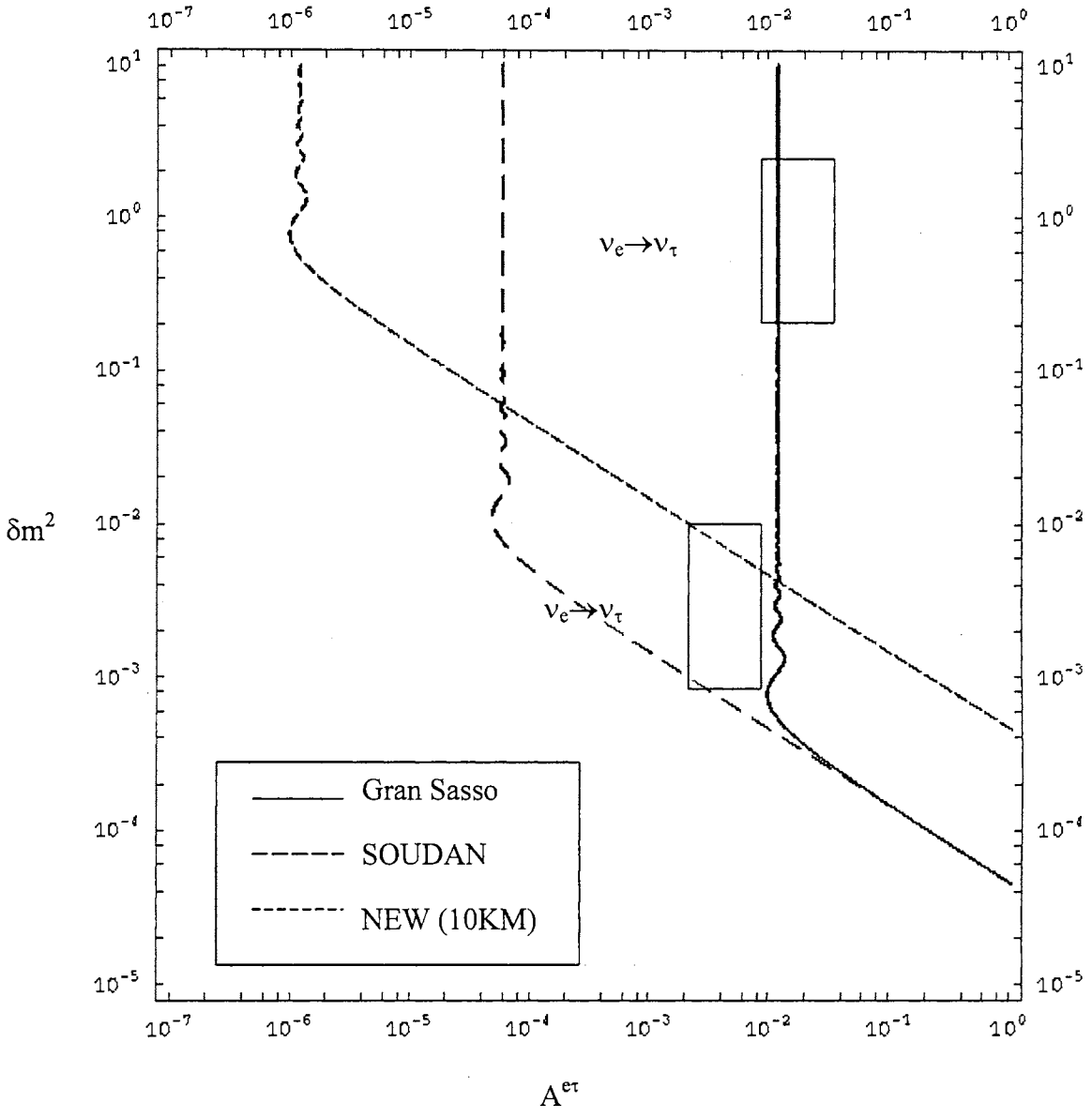

Figure 8. The $\nu_e \rightarrow \nu_\tau$ predicted parameter space for the M2A-SAM model.

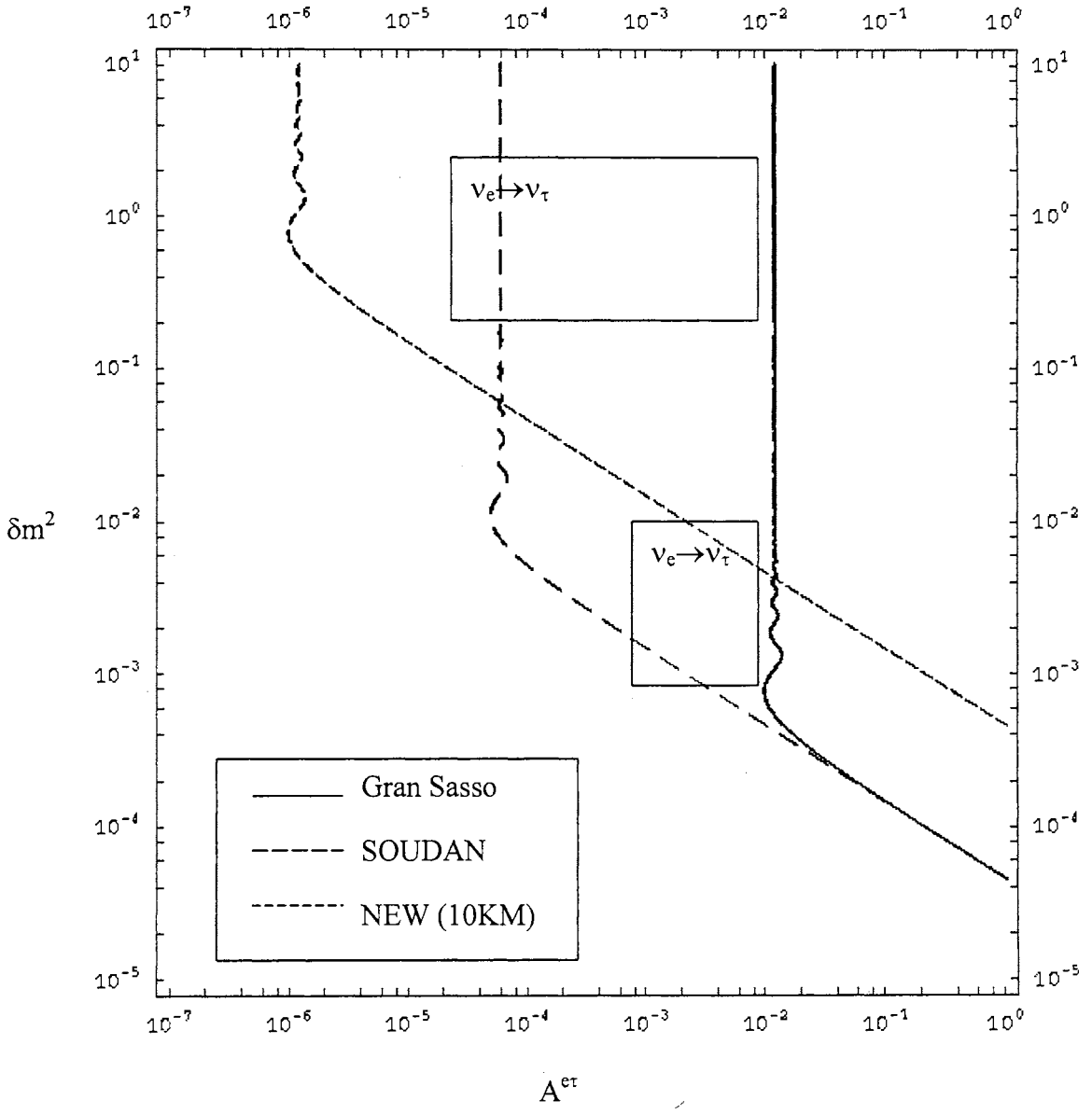

Figure 9. The $\nu_e \rightarrow \nu_\tau$ predicted parameter space for the M5A-SAM model.

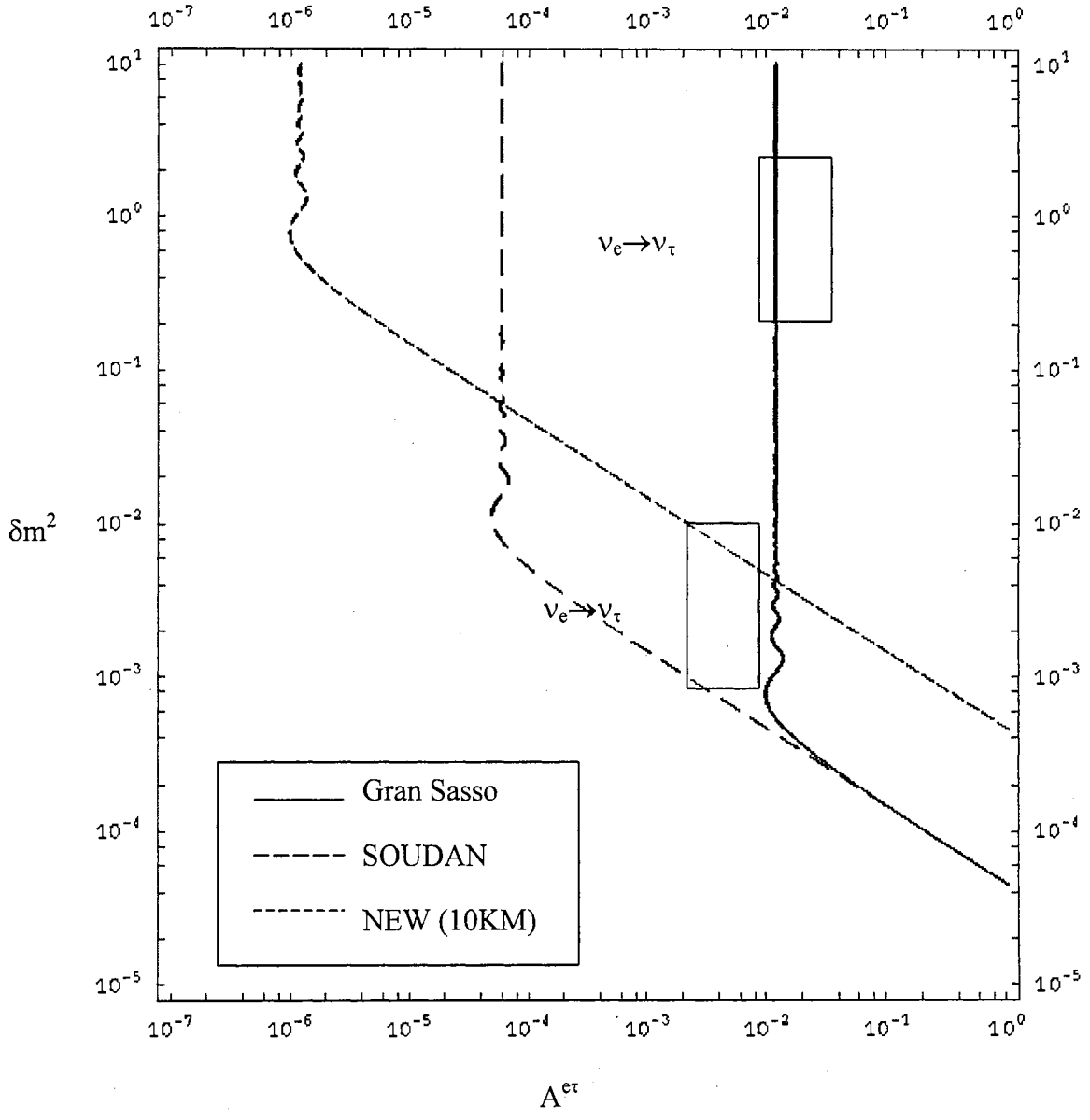

Figure 10. The $\nu_e \rightarrow \nu_\tau$ predicted parameter space for the M6A-SAM model.

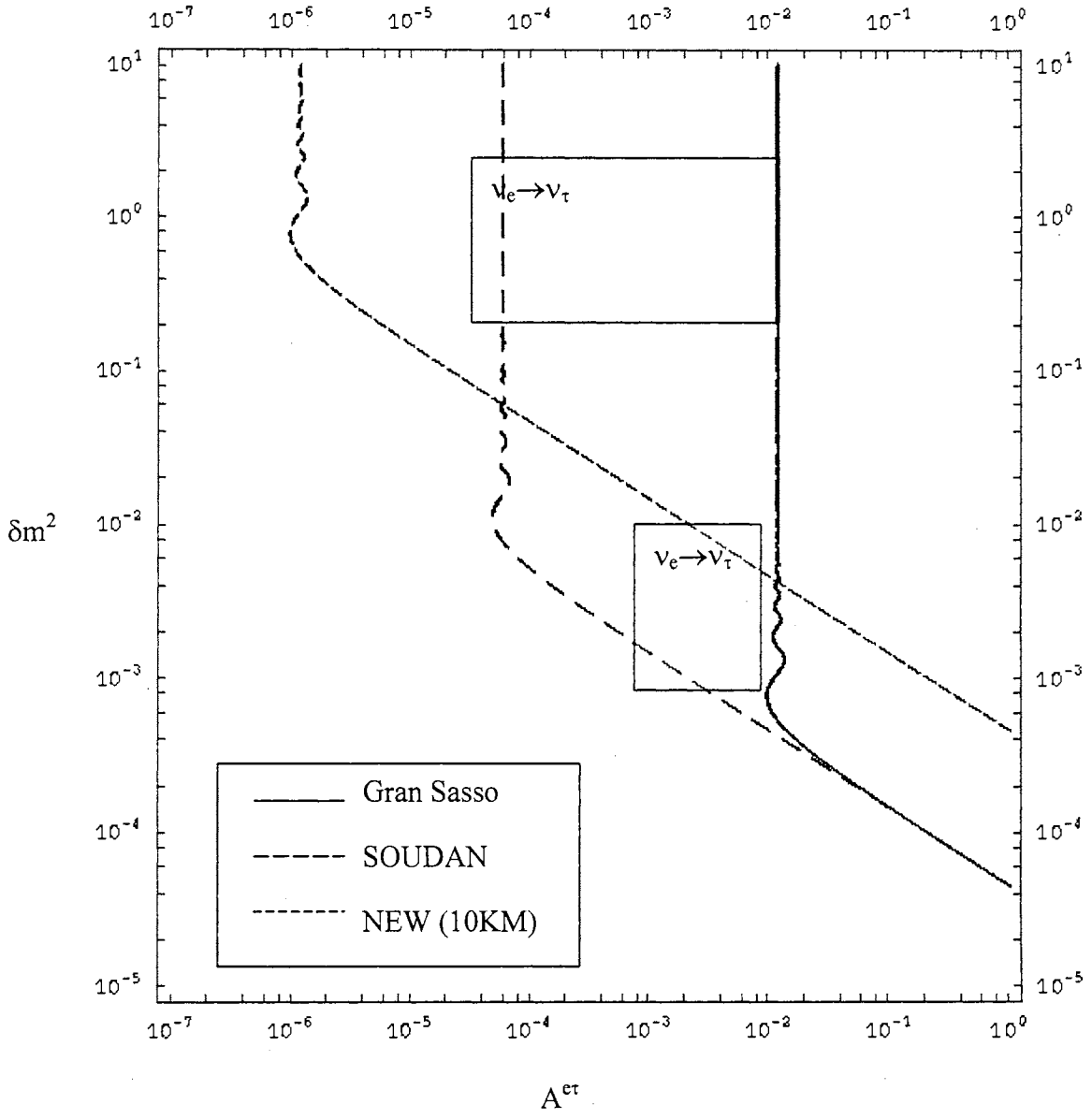

Figure 11. The $\nu_e \rightarrow \nu_\tau$ predicted parameter space for the M9A-SAM model.

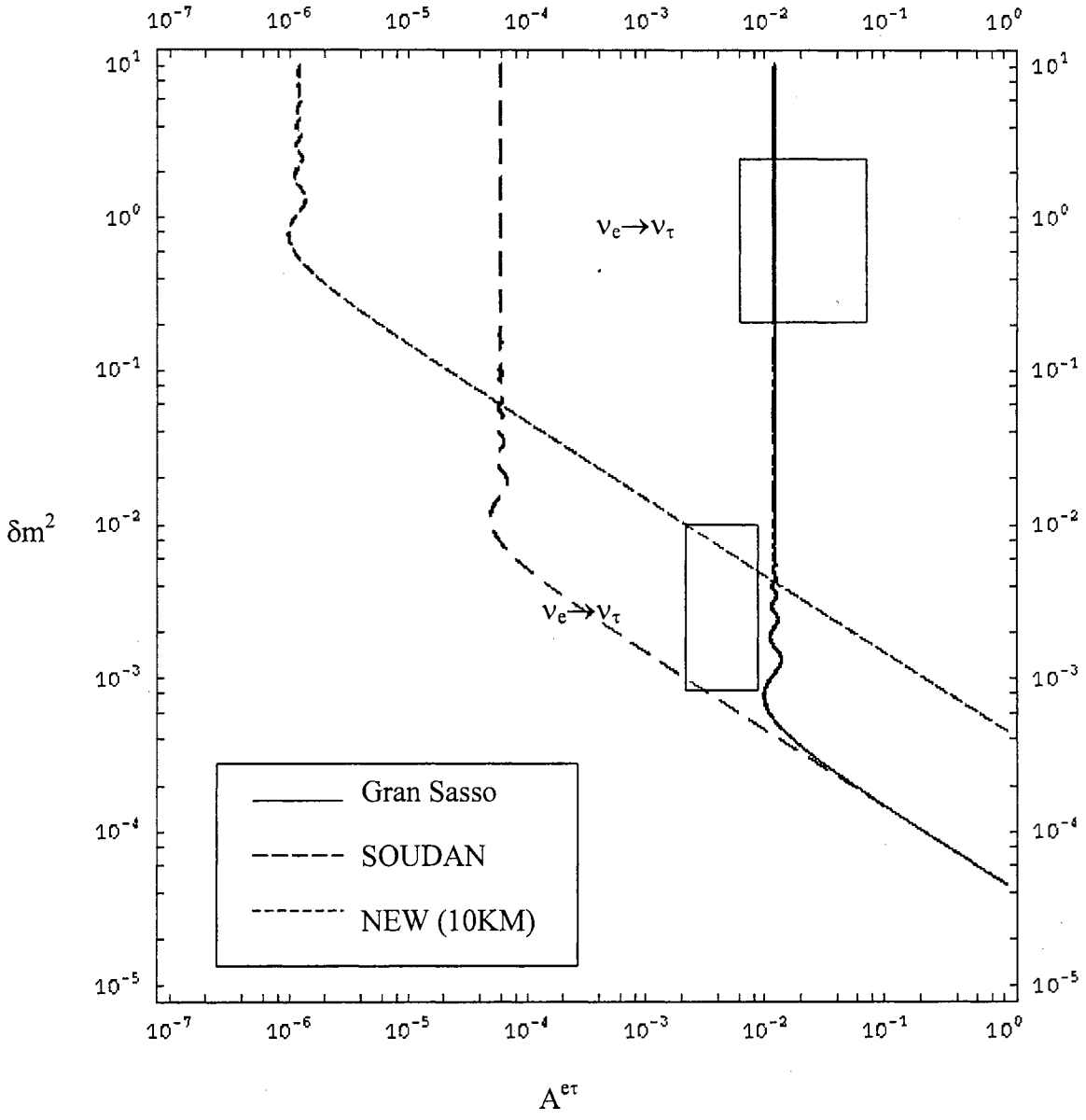

Figure 12. The $\nu_e \rightarrow \nu_\tau$ predicted parameter space for the M10A-SAM model.

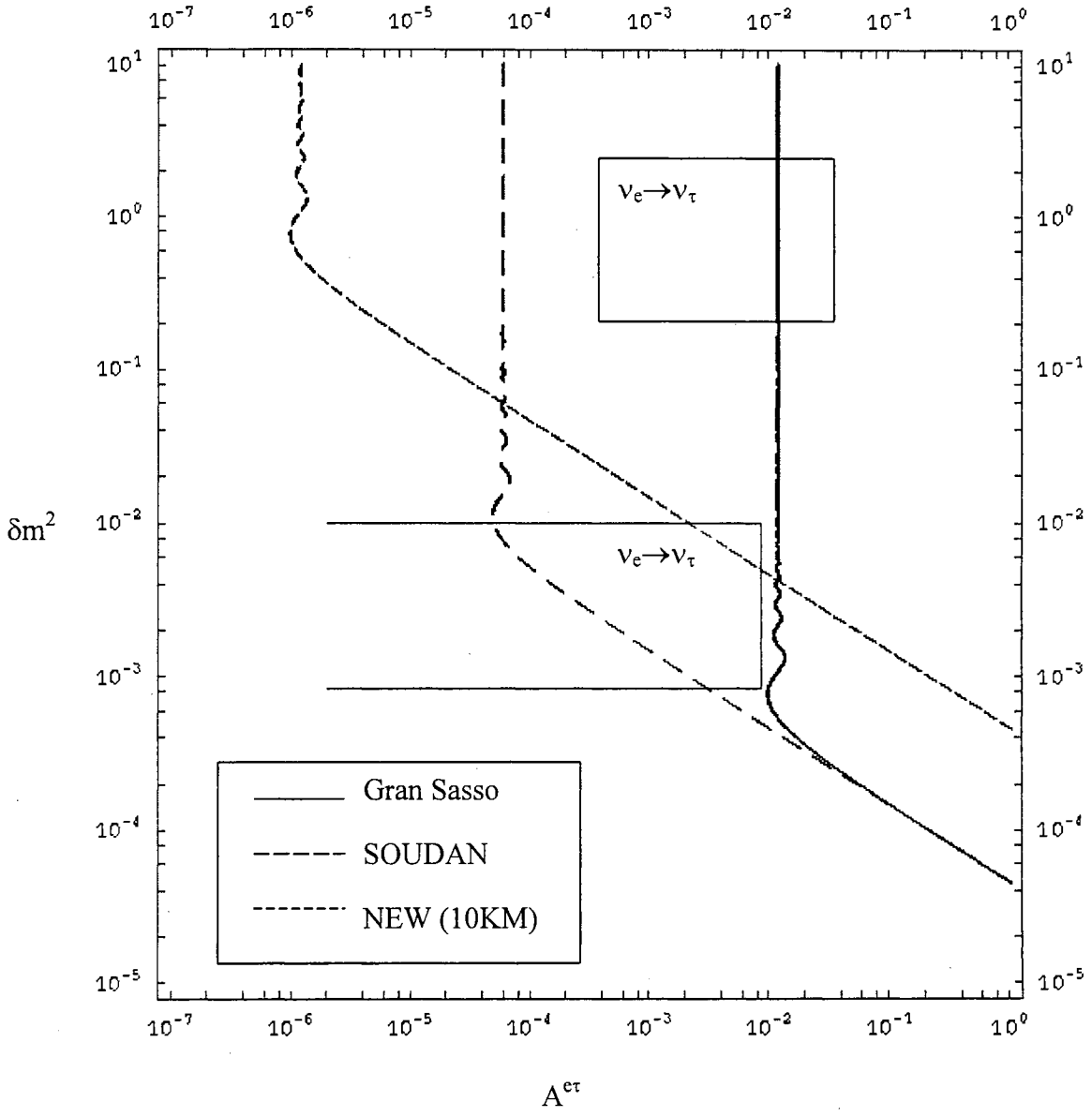

Figure 13. The $\nu_e \rightarrow \nu_\tau$ predicted parameter space for the M21A-SAM model.

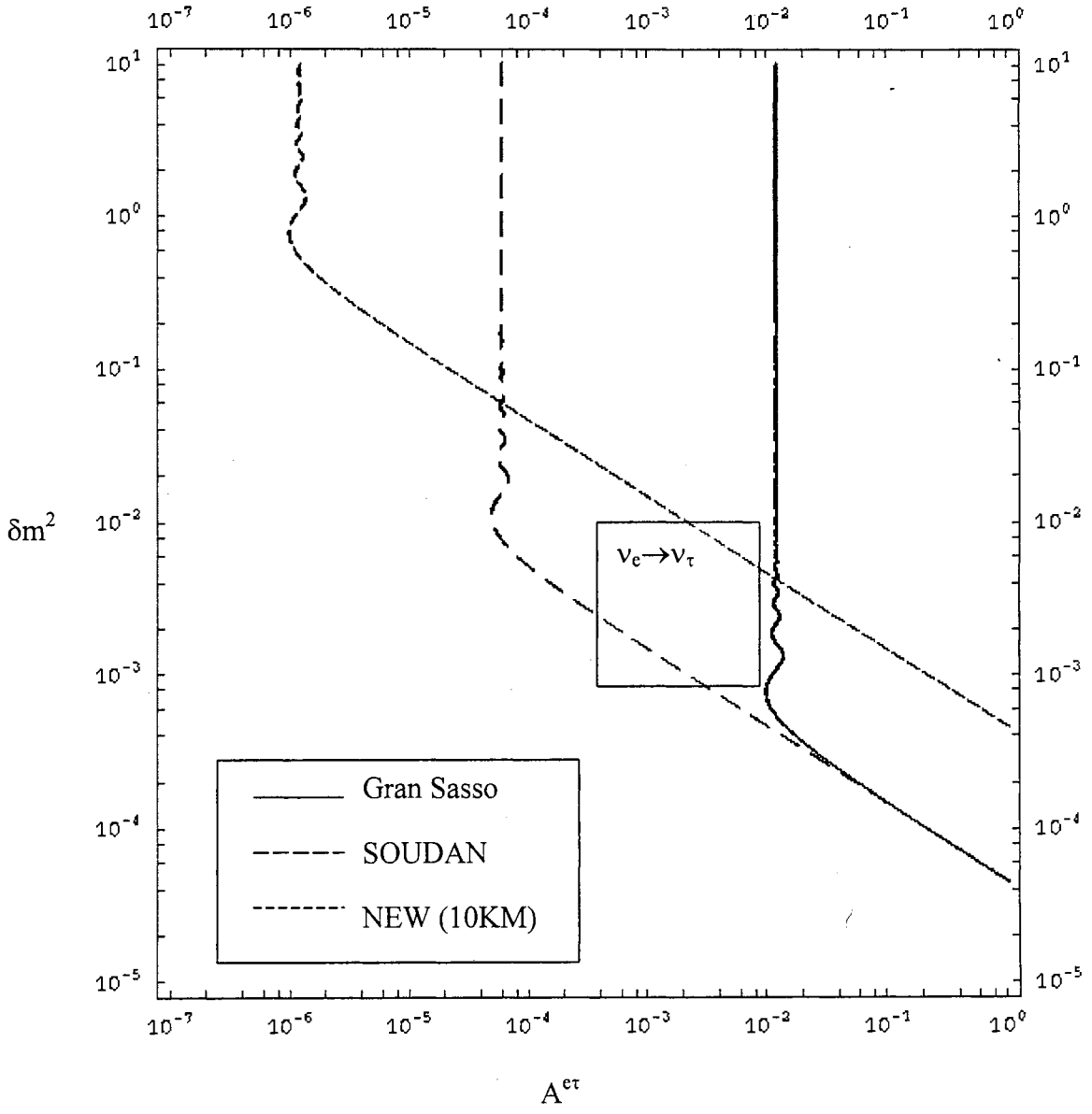

Figure 14. The $\nu_e \rightarrow \nu_\tau$ predicted parameter space for the M22A-SAM model.

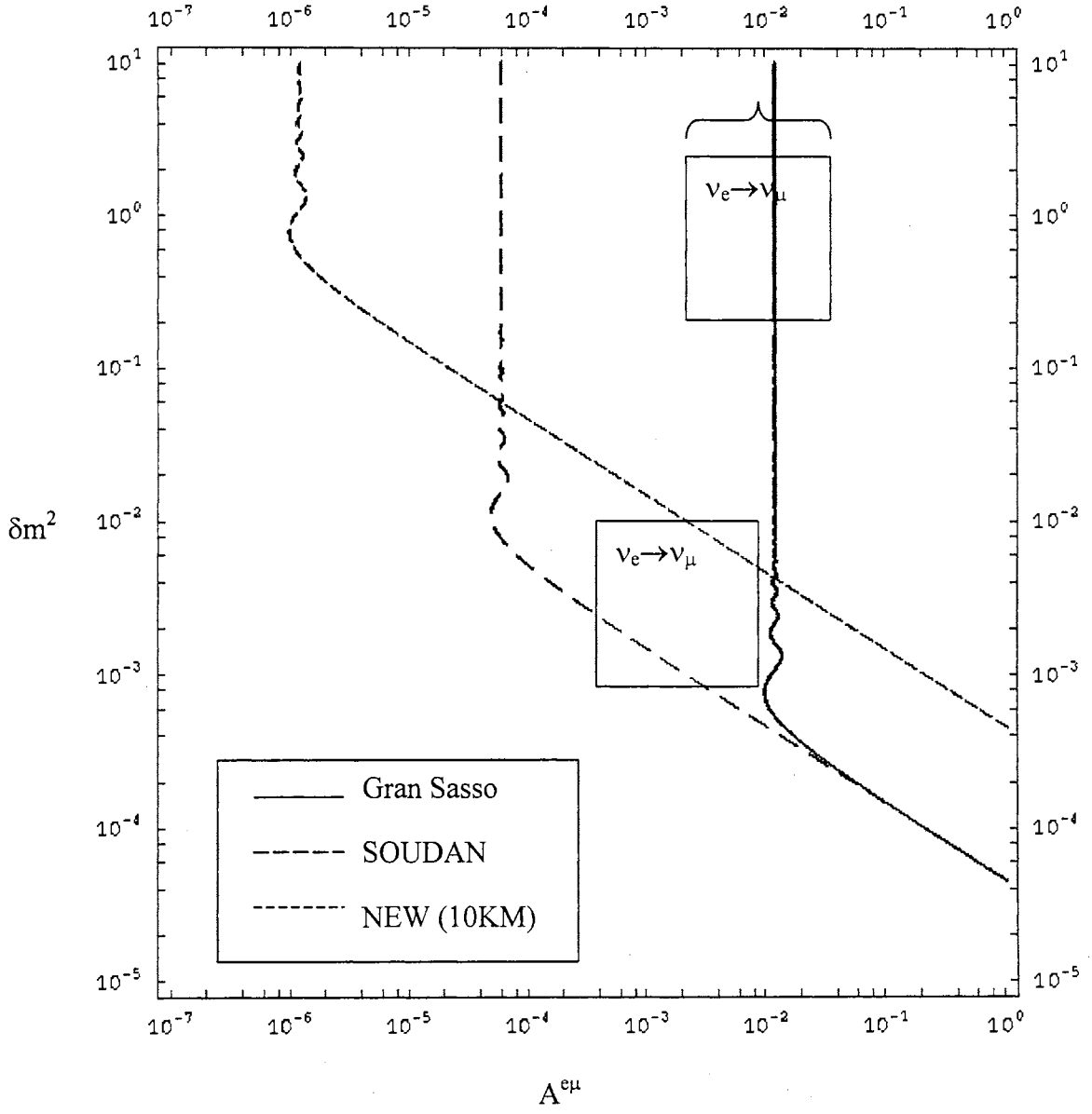

Figure 15. The $\nu_e \rightarrow \nu_\mu$ predicted parameter space for the M1 matrix.

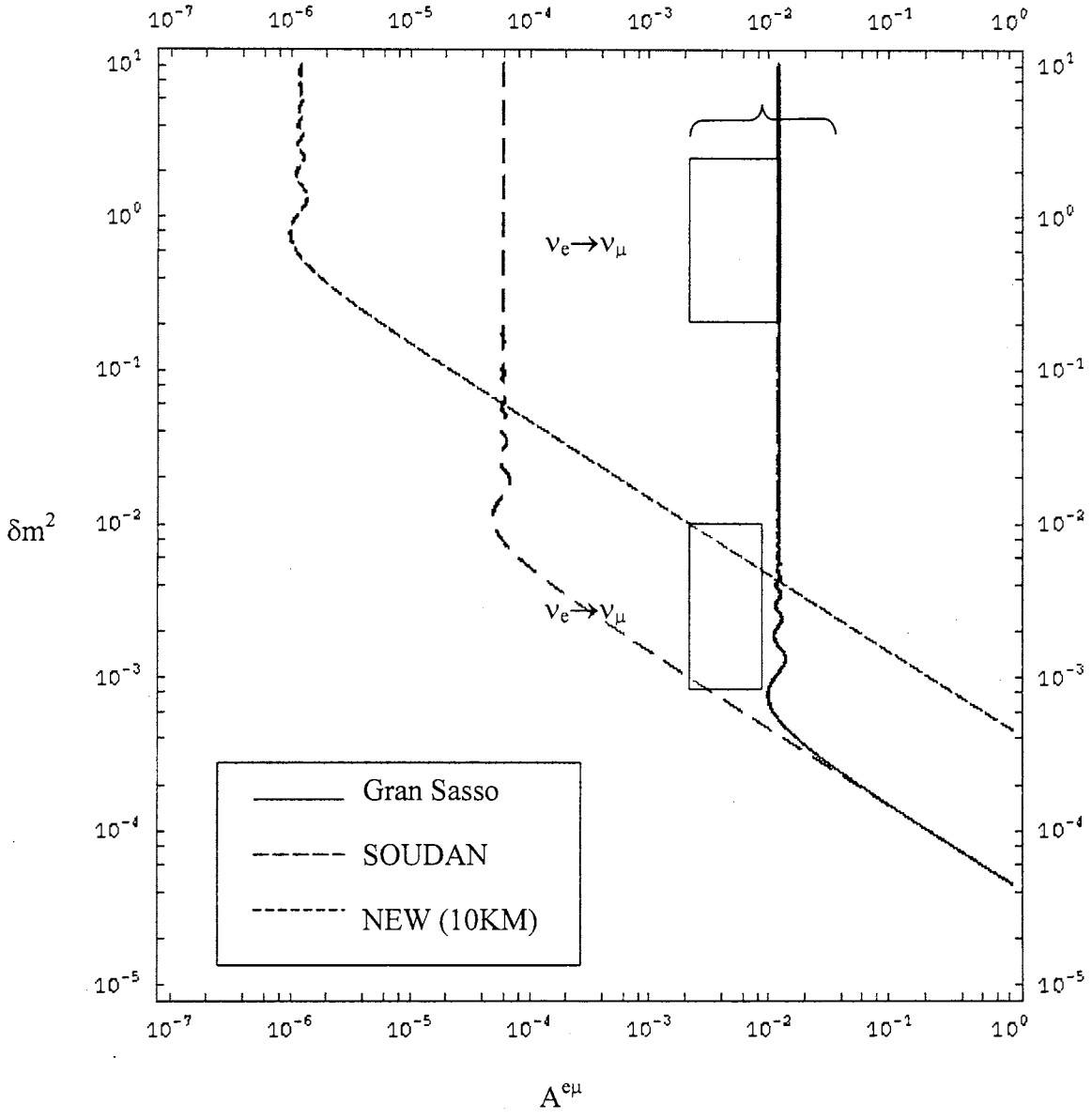

Figure 16. The $\nu_e \rightarrow \nu_\mu$ predicted parameter space for the M2 matrix.

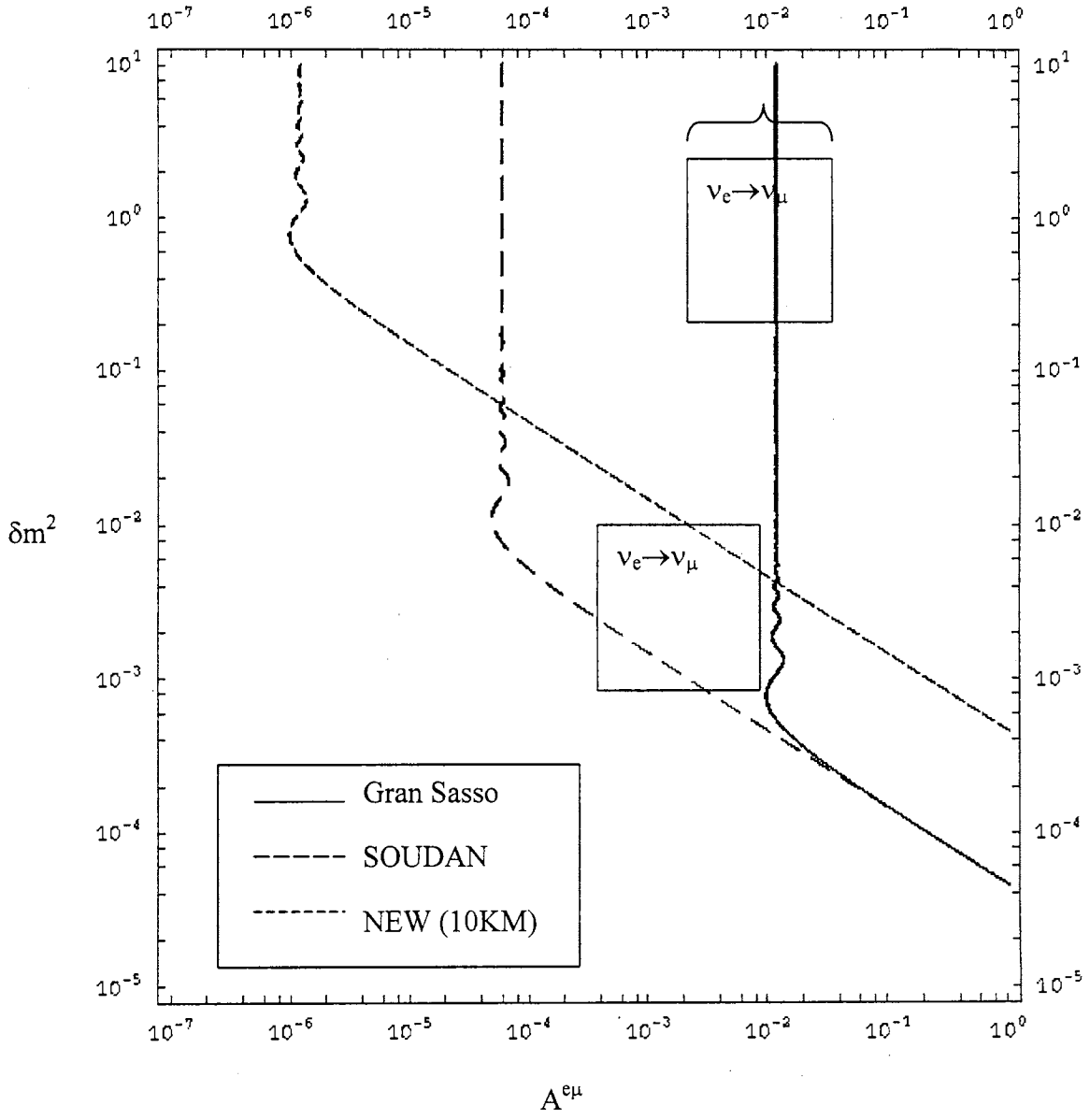

Figure 17. The $\nu_e \rightarrow \nu_\mu$ predicted parameter space for the M5 matrix.

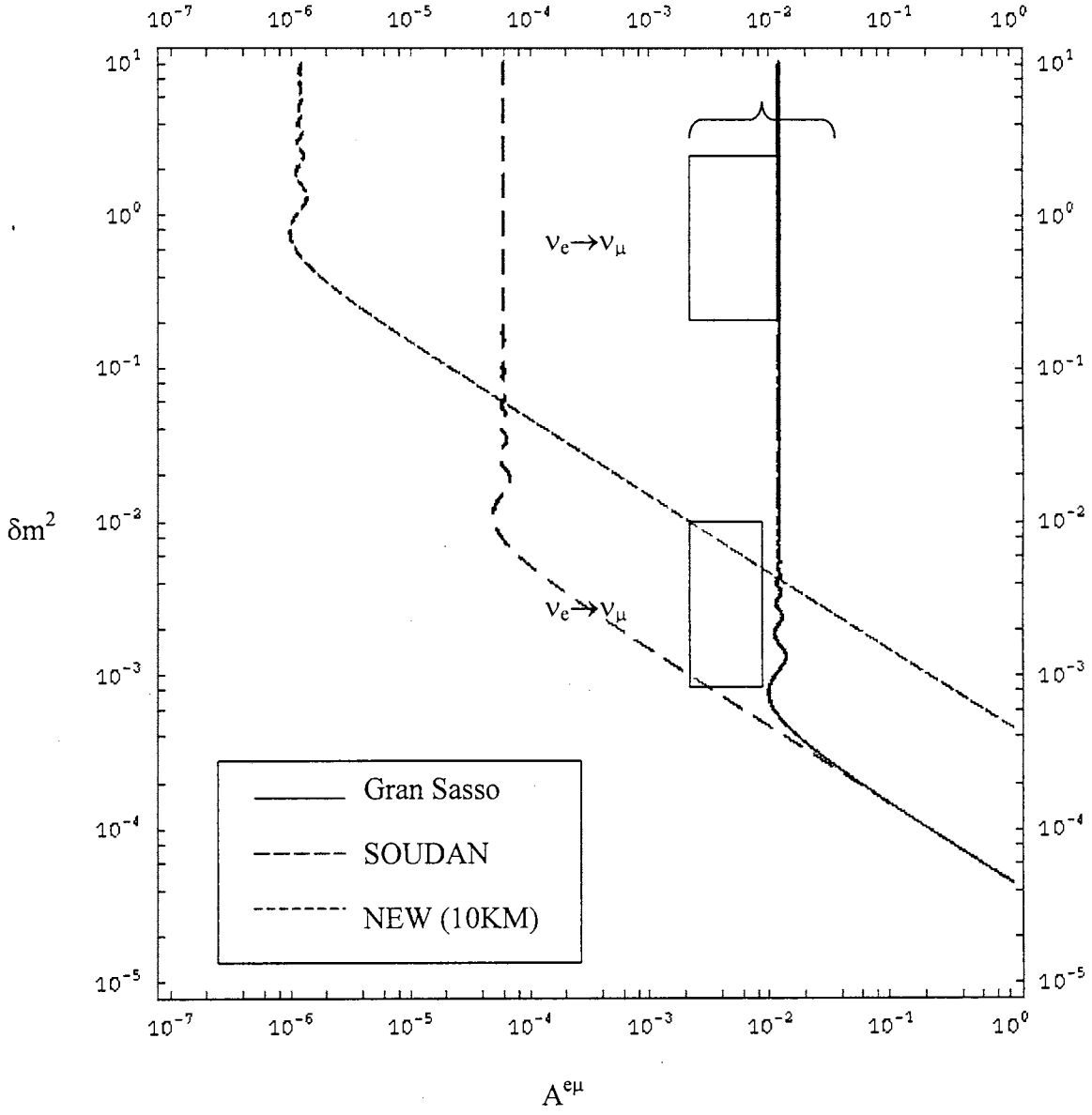

Figure 18. The $\nu_e \rightarrow \nu_\mu$ predicted parameter space for the M6 matrix.

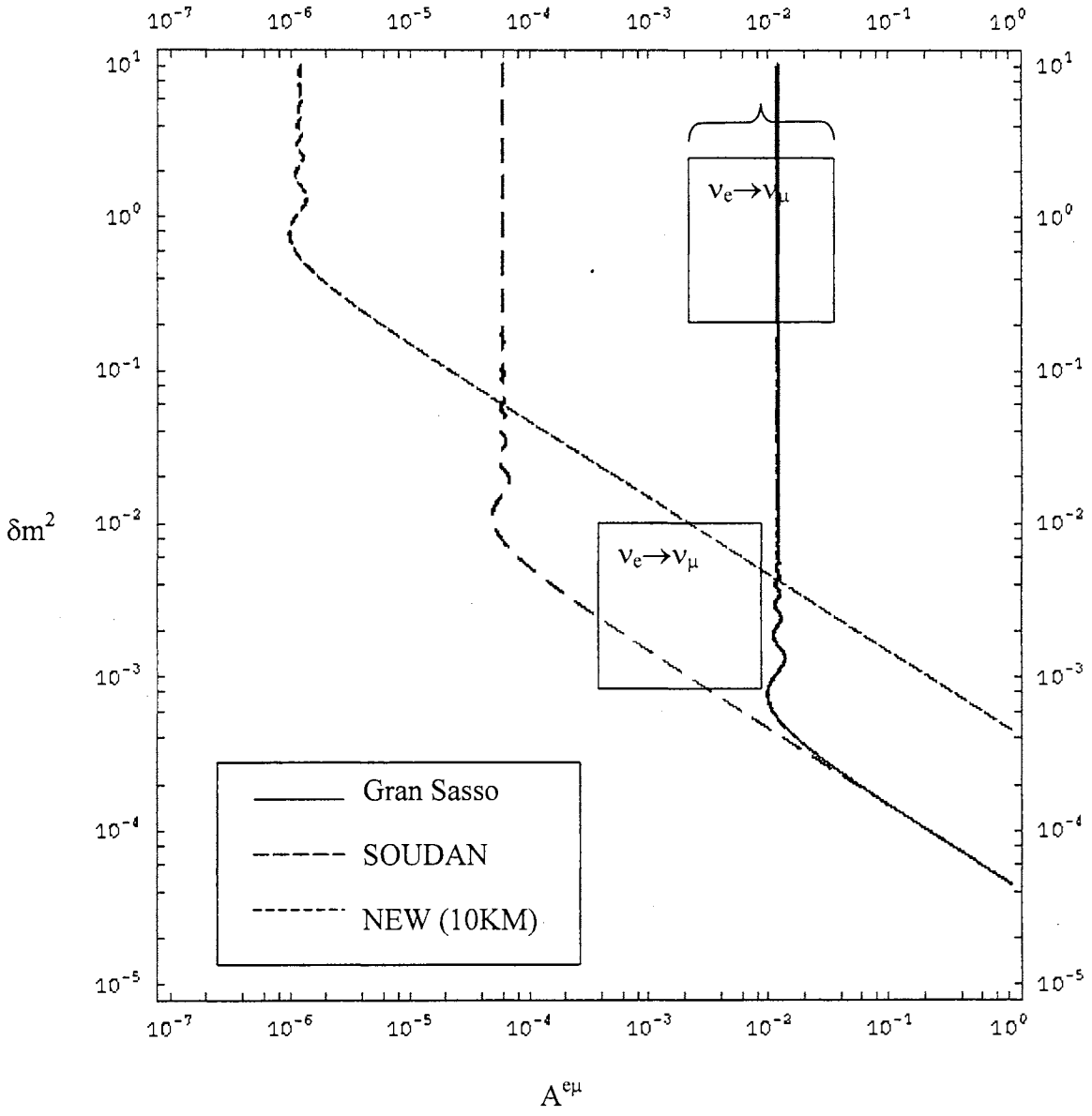

Figure 19. The $\nu_e \rightarrow \nu_\mu$ predicted parameter space for the M9 matrix.

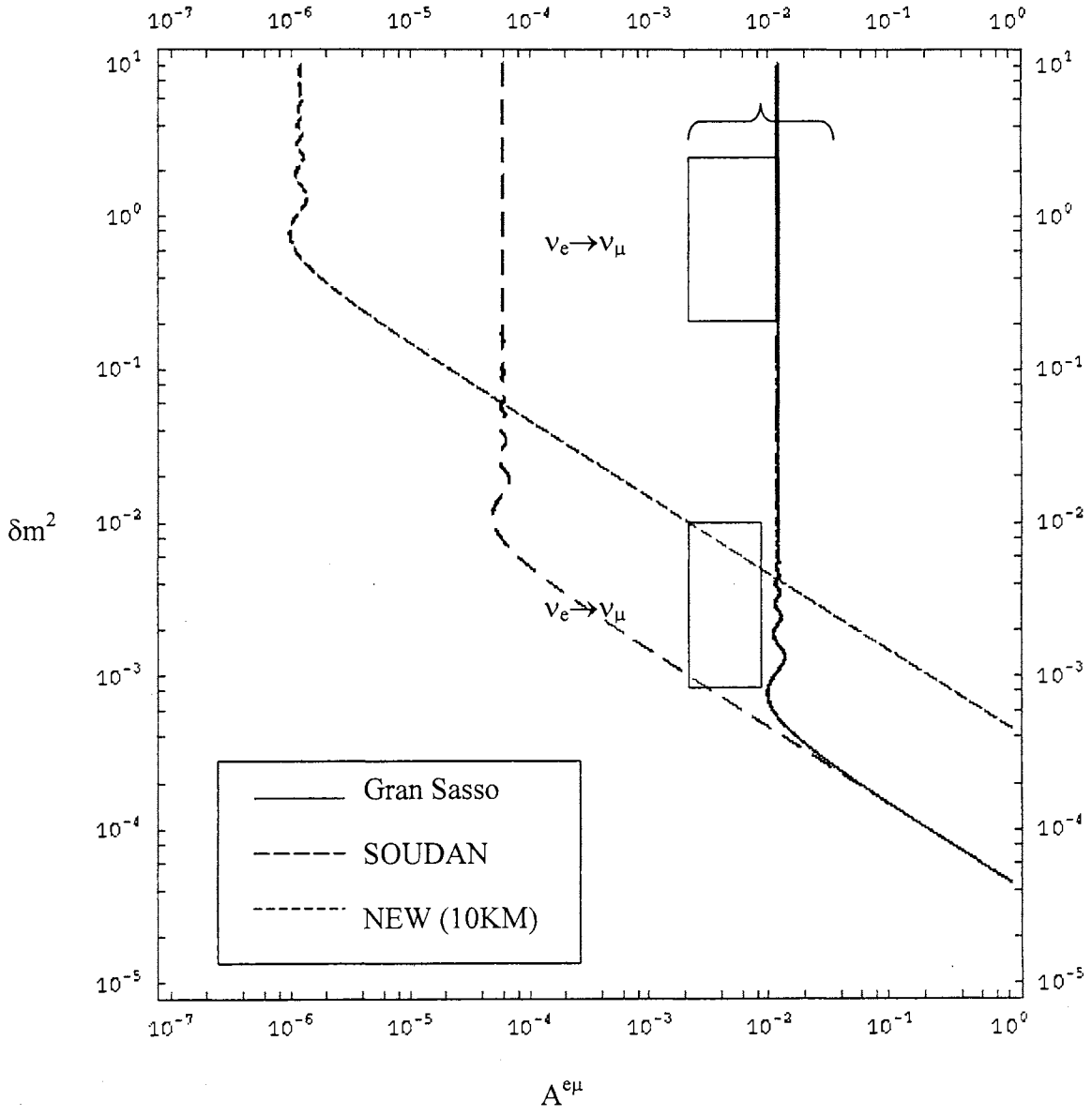

Figure 20. The $\nu_e \rightarrow \nu_\mu$ predicted parameter space for the M10 matrix.

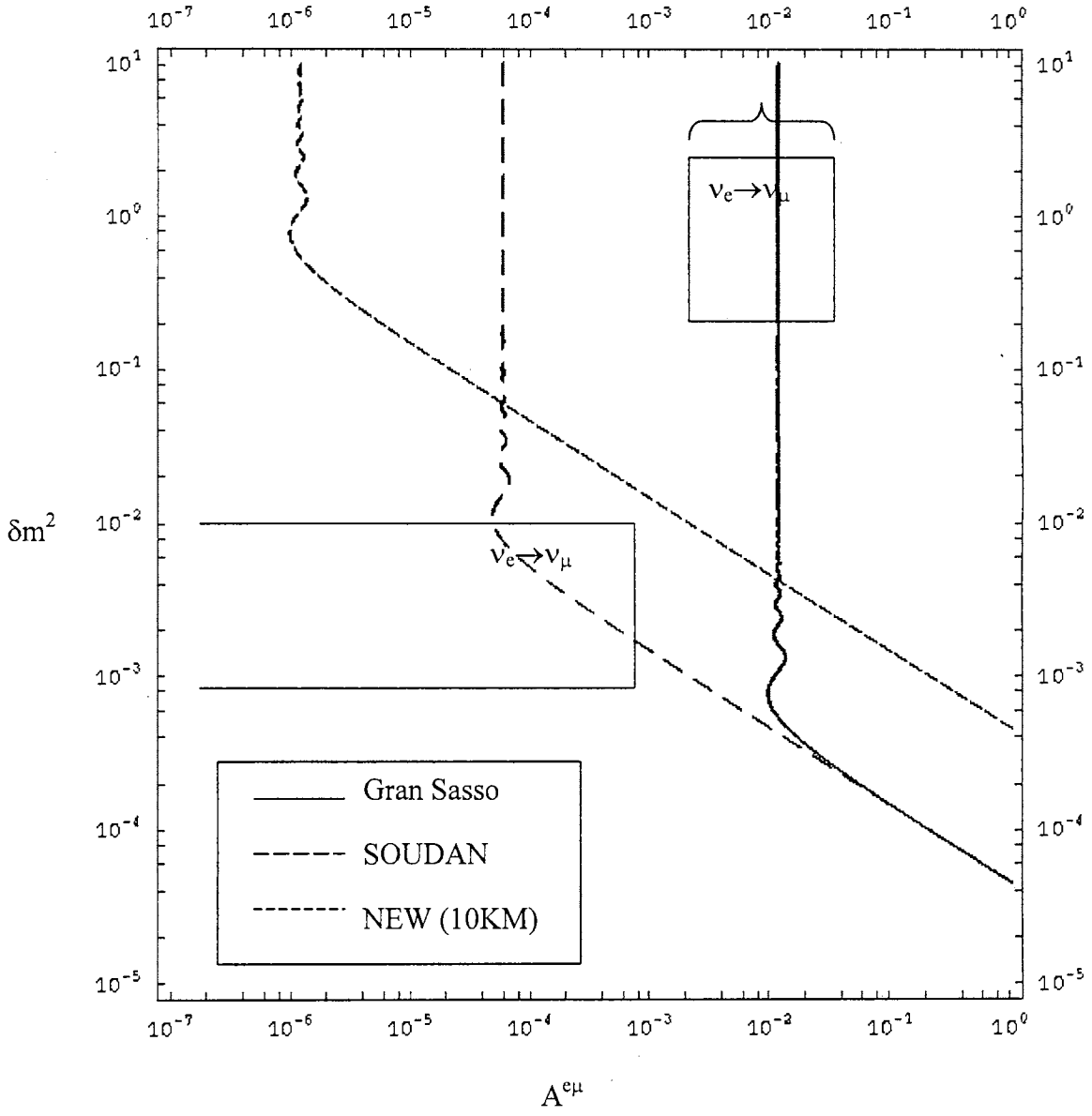

Figure 21. The $\nu_e \rightarrow \nu_\mu$ predicted parameter space for the M21 matrix.

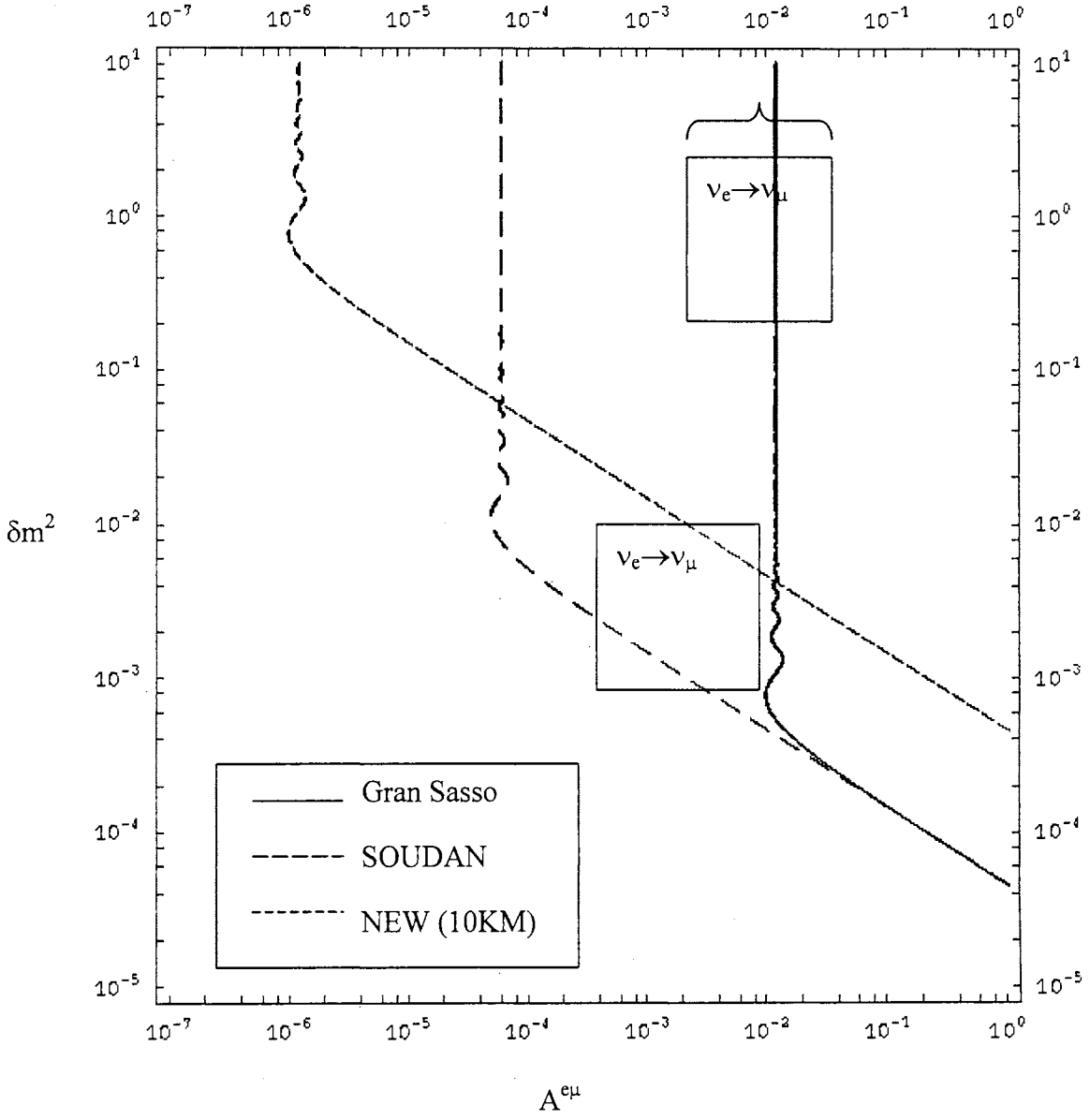

Figure 22. The $\nu_e \rightarrow \nu_\mu$ predicted parameter space for the M22 matrix.

VITA

Stephen C. Gibbons

Candidate for the degree of

Doctor of Philosophy

Thesis: SPIN 3/2 QUARK PRODUCTION/DETECTION AND ANALYSIS OF 147 FOUR NEUTRINO MASS MATRICES

Major Field: Physics

Biographical:

Personal Data: Born in Wichita, Kansas, On May 10, 1956, the son of Larry and Louis Gibbons. Married, with one child, Paul Timothy Gibbons.

Education: Received a Bachelor of Science degree in Physics and a Master of Science degree from Wichita State University, Wichita, Kansas in 1983 and 1990 respectively. Completed the Requirements for the Doctor of Philosophy degree at Oklahoma State University in May, 1999.

Experience: I've been teaching as a Teaching Assistant for nine years at Oklahoma State University. I've been the Physics Professor at Newman University in Wichita, Kansas since Fall, 1998.